

## Supplement: Designed proteins assemble antibodies into modular nanocages

Robby Divine<sup>1,2</sup>, Ha V. Dang<sup>1</sup>, George Ueda<sup>1,2</sup>, Jorge A. Fallas<sup>1,2</sup>, Ivan Vulovic<sup>1,2</sup>, William Sheffler<sup>2</sup>, Shally Saini<sup>1,3</sup>, Yan Ting Zhao<sup>1,3,4</sup>, Infencia Xavier Raj<sup>1,3</sup>, Peter A. Morawski<sup>5</sup>, Madeleine F. Jennewein<sup>6</sup>, Leah J. Homad<sup>6</sup>, Yu-Hsin Wan<sup>6</sup>, Marti R. Tooley<sup>2</sup>, Franzika Seeger<sup>1,2</sup>, Ali Etemadi<sup>2,7</sup>, Mitchell L. Fahning<sup>5</sup>, James Lazarovits<sup>1,2</sup>, Alex Roederer<sup>2</sup>, Alexandra C. Walls<sup>1</sup>, Lance Stewart<sup>2</sup>, Mohammadali Mazloomi<sup>7</sup>, Neil P. King<sup>1,2</sup>, Daniel J. Campbell<sup>5</sup>, Andrew T. McGuire<sup>6,8</sup>, Leonidas Stamatatos<sup>6,8</sup>, Hannele Ruohola-Baker<sup>1,3</sup>, Julie Mathieu<sup>3,9</sup>, David Veessler<sup>1</sup>, David Baker<sup>1,2,10\*</sup>

10

### Affiliations:

<sup>1</sup> Department of Biochemistry, University of Washington, Seattle, WA 98195, USA.

<sup>2</sup> Institute for Protein Design, University of Washington, Seattle, WA 98195, USA.

<sup>3</sup> Institute for Stem Cell and Regenerative Medicine, University of Washington, Seattle, WA 98109, USA.

<sup>4</sup> Oral Health Sciences, School of Dentistry, University of Washington, Seattle, WA 98195, USA.

<sup>5</sup> Benaroya Research Institute, Seattle, WA 98101, USA

<sup>6</sup> Fred Hutchinson Cancer Research Center, Vaccines and Infectious Diseases Division, Seattle, WA, USA

<sup>7</sup> Medical Biotechnology Department, School of Advanced Technologies in Medicine, Tehran University of Medical Sciences (TUMS), Tehran, Iran.

<sup>8</sup> University of Washington, Department of Global Health, Seattle, WA, USA

<sup>9</sup> Department of Comparative Medicine, University of Washington, Seattle, WA 98195, USA.

<sup>10</sup> Howard Hughes Medical Institute, University of Washington, Seattle, WA 98195, USA.

25 \*Corresponding author. E-mail: [dabaker@uw.edu](mailto:dabaker@uw.edu)

**This document includes:**

1. Materials and methods
2. Figures S1-S11
3. Tables S1-S15
- 5 4. Supplementary text
5. Full reference list (1-62)

**Materials and Methods**

**Computational design and testing of Fc-binder helical repeat protein (DHR79-FcB)**

10           The crystal structure of the B-domain from *S. aureus* protein A in complex with Fc fragment (PDB ID: 1L6X) was relaxed with structure factors using Phenix Rosetta (45, 46). Briefly, the RosettaScripts MotifGraft mover was used to assess suitable solutions to insertions of the protein A binding motif extracted from 1L6X into a previously reported designed helical repeat protein (DHR79) (19). Specifically, a

15           minimal protein A binding motif was manually defined and extracted and used as a template for full backbone alignment of DHR79 while retaining user-specified hotspot residues that interact with the Fc domain in the crystal structure at the Fc/DHR interface and retaining native DHR residues in all other positions. The MotifGraft alignment was followed by 5 iterations of FastDesign and 5 iterations of FastRelax in which the DHR

20           side chain and backbone rotamers were allowed to move while the Fc context was completely fixed. The best designs were selected based on a list of heuristic filter values. Fig. S1a shows the design model of DHR79-FcB.

          Designs were initially assessed via yeast surface display binding to biotinylated Fc protein; yeast display procedures followed previously-published protocols (47). Upon

confirmation of a qualitative binding signal, the design was cloned into a pET29b expression vector with a C-terminal His-tag. The protein was expressed in BL21 DE3 in autoinduction medium (6 g tryptone, 12 g yeast extract, 10 mL 50×M, 10 mL 50×5052, 1 mL 1M MgSO<sub>4</sub>, 100 μL Studier Trace metals, 50 μg kanamycin antibiotic, brought to a final volume of 500 mL using filtered water) for 20 hours at 27°C at 225 rpm; 50×M, 50×5052, and Studier trace metals were prepared according to previously-published recipes (48). Cells were resuspended in lysis buffer (20mM Tris, 300mM NaCl, 30mM imidazole, 1mM phenylmethylsulfonyl fluoride (PMSF), 5% glycerol (v/v), pH 8.0) and lysed using a microfluidizer at 18000 PSI. Soluble fractions were separated via centrifugation at 24,000×g. IMAC with Ni-NTA batch resin was used for initial purification; briefly, nickel-nitrilotriacetic acid (Ni-NTA) resin was equilibrated with binding buffer (20mM Tris, 300mM NaCl, 30mM imidazole, pH 8.0), soluble lysate was poured over the columns, columns were washed with 20 column volumes (CVs) of binding buffer, and eluted with 5 CVs of elution buffer (20mM Tris, 300mM NaCl, 500mM imidazole, pH 8.0). Size exclusion chromatography (SEC) with a Superdex 200 column was used as the polishing step (Fig. S1b). SEC buffer was 20 mM Tris/HCl pH 7.4, 150 mM NaCl.

Affinity of DHR79-FcB to biotinylated IgG1 and biotinylated Fc protein bound to streptavidin plates was assessed using Octet Biolayer Interferometry (BLI). Data was fit using a 1:1 binding mode. Both 1:1 and 2:1 binding stoichiometries were assessed, and it was determined that the 1:1 binding mode better accounted for the noise in the experiment. This was tested on the Fc binder monomer before any Fc binder-oligomer

fusions were made. DHR79-FcB exhibits a 71.7 nM affinity to IgG1 (full antibody) and a 113 nM affinity to the IgG1 Fc protein (Fig S1c).

### Computational Design of Antibody Nanocages

5           Input .pdb files were compiled to use as building blocks for the generation of antibody cages. For the protein A binder model, the Domain D from *Staphylococcus aureus* Protein A (PDB ID 1DEE) was aligned to the B-domain of protein A bound to Fc (PDB ID: 1L6X) (18, 45). The other Fc-binding design structure, where protein A was grafted onto a helical repeat protein, was also modeled with Fc from 1L6X. PDB file  
10           models for monomeric helical repeat protein linkers (42) and cyclic oligomers (2 C2s, 3 C3s, 1 C4, and 2 C5s) that had at least been validated via SAXS were compiled from previous work from our lab (19–21). Building block models were manually inspected to determine which amino acids were suitable for making fusions without disrupting existing protein-protein interfaces.

15           These building blocks were used as inputs, along with the specified geometry and fusion orientation, into the alpha helical fusion software (“WORMS,” ran using instructions provided at <https://github.com/willsheffler/worms>; also see Supplementary Text for a description on how to operate WORMS) (14, 15). Fusions were made by overlapping helical segments at all possible allowed amino acid sites. Fusions are then  
20           evaluated for deviation for which the cyclic symmetry axes intersect according to the geometric criteria: D2, T32, O32, O42, I32, and I52 intersection angles are 45.0°, 54.7°, 35.3°, 45.0°, 20.9°, and 31.7°, respectively (22) with angular and distance tolerances of at most 5.7° and 0.5 Å respectively. Post-fusion .pdb files were manually filtered to

ensure that the N-termini of the Fc domains are facing outwards from the cage, so that the Fabs of an IgG would be external to the cage surface. Sequence design was performed using Rosetta symmetric sequence design (SymPackRotamersMover in RosettaScripts) on residues at and around the fusion junctions (49), with a focus on maintaining as many of the native residues as possible. Residues were redesigned if they clashed with other residues, or if their chemical environment was changed after fusion (e.g. previously-core facing residues were now solvent-exposed). Index residue selectors were used to prevent design at Fc residue positions. See Supplemental Materials 4 for an example .xml file used in post-fusion design.

10

## **Protein expression for AbC-forming designs and Fc constructs**

### *Bacterial expression of AbC-forming designs*

Genes were codon optimized for bacterial expression of each designed AbC forming oligomer, with a C-terminal glycine/serine linker and 6× C-terminal histidine tag appended. Synthetic genes were cloned into pet29b+ vectors between NdeI and XhoI restriction sites; the plasmid contains a kanamycin-resistant gene and T7 promoter for protein expression. Plasmids were transformed into chemically competent Lemo21(DE3) *E. coli* bacteria using a 15-second heat shock procedure as described by the manufacturer (New England Biolabs). Transformed cells were added to auto-induction expression media, as described above, and incubated for 16 hours at 37°C and 200 rpm shaking (48). Cells were pelleted by centrifugation at 4000×g and resuspended in lysis buffer (150 mM NaCl, 25 mM Tris-HCl, pH 8.0, added protease inhibitor and DNase). Sonication was used to lyse the cells at 85% amplitude, with 15

second on/off cycles for a total of 2 minutes of sonication time. Soluble material was separated by centrifugation at 16000×g. IMAC was used to separate out the His-tagged protein in the soluble fraction as described above. IMAC elutions were concentrated to approximately 1 mL using 10K MWCO spin concentrators, filtered through a 0.22 μM spin filter, and run over SEC as a final polishing step (SEC running buffer: 150 mM NaCl, 25 mM Tris-HCl, pH 8.0).

### *Production of Fc and Fc-fusions*

Synthetic genes were optimized for mammalian expression and subcloned into the CMV/R vector (VRC 8400) (50). XbaI and AvrII restriction sites were used for insertion of the target gene (Fc, GFP-Fc, RFP-Fc, or A1F-Fc). Gene synthesis and cloning was performed by Genscript. Expi293F cells were grown in suspension using Expi293 Expression Medium (Thermo Fisher Scientific) at 150 RPM, 5% CO<sub>2</sub>, 70% humidity, 37°C. At confluency of ~2.5×10<sup>6</sup> cells/mL, the cells were transfected with the vector encoding the Fc or Fc-fusion (1000 μg per 1 L of cells) using PEI MAX (Polysciences) as a transfection reagent. Cells were incubated for 96 hours, after which they were spun down by centrifugation (4,000×g, 10 min, 4 °C) and the protein-containing supernatant was further clarified by vacuum-filtration (0.45 μm, Millipore Sigma). In preparation of nickel-affinity chromatography steps, 50 mM Tris, 350 mM NaCl, pH 8.0 was added to the clarified supernatant. For each liter of supernatant, 4 mL of Ni Sepharose excel resin (GE) was added to the supernatant, followed by overnight shaking at 4 °C. After 16-24 h, resin was collected and separated from the mixture and washed twice with 50 mM Tris, 500 mM NaCl, 30 mM imidazole, pH 8.0 prior to elution

of desired protein with 50 mM Tris, 500 mM NaCl, 300 mM imidazole, pH 8.0. Eluates were purified by SEC using a Superdex 200 Increase column.

### **Structural evaluation of AbC-forming designs**

5 Designs that produced monodisperse SEC peaks around their expected retention volume were combined with Fc from human IgG1. Cage components were incubated at 4°C for at minimum 30 minutes. 100 mM L-arginine was added during the assembly to AbCs formed with the i52.6 design, as this was observed to maximize the formation of the designed AbC I52 and prevent the formation of visible “crashed out” aggregates  
10 (23). Fc-binding and cage formation were confirmed via SEC; earlier shifts in retention time (compared to either component run alone) show the formation of a larger structure. NS-EM was used as described below to confirm the structures of designs that passed these steps.

For confirming AbC structures with intact IgGs, human IgG1 (hIgG1) was  
15 combined with AbC-forming designs following the same protocol for making Fc cages. This assembly procedure was also followed for all IgG or Fc-fusion AbCs reported hereafter. The data in Figure 2d-e shows AbCs formed with the  $\alpha$ -DR5 antibody AMG-655 (23) for the following designs: d2.3, d2.4, d2.7, t32.4, t32.8, o42.1, and i52.3. The data for the i52.6 design shown in Figure 2d-e is from AbCs formed with the hIgG1  
20 antibody mpe8 (51); this was simply due to limited AMG-655 availability at the time of the experiment and not a reflection on i52.6/AMG-655 assembly competency. Tables S12 and S13 show the list of IgGs and Fc fusions that have been formed into AbCs. Table S14 lists the amino acid sequences of all successful AbC-forming designs; Table

S15 lists the amino acid sequences of Fc and Fc-fusions used in the following experiments.

## SAXS

5            Samples were prepared for small-angle X-ray scattering (SAXS) analysis by first expressing and purifying AbCs with Fc as described above. Fc AbCs were sized into 150 mM NaCl and 25 mM Tris-HCl at pH 8.0. Fractions corresponding to the Fc AbC peak off SEC were combined and glycerol was added at 2% final concentration. Samples were concentrated to between 1-3 mg/mL using a 10K molecular weight cut-  
10 off (MWCO) benchtop spin concentrator. The flow-through was used as a blank for buffer subtraction during SAXS analysis. Proteins were then passed through a 0.22 µm syringe filter (Millipore). These proteins and buffer blanks were shipped to the SIBYLS High Throughput SAXS Advanced Light Source in Berkeley, California to obtain scattering data (25). Scattering traces were fit to theoretical models using the FOXS  
15 server (<https://modbase.compbio.ucsf.edu/foxs/>) (24).

### *NS-EM specimen preparation and data collection of Fc and IgG AbCs*

For all samples except o42.1 Fc and i52.3 Fc, 3.0 µL of each SEC-purified sample between 0.008- 0.014 mg/mL in TBS pH 8.0 was applied onto a 400-mesh or  
20 200-mesh Cu grid glow-discharged carbon-coated copper grids for 20s, followed by 2× application of 3.0 µL 2% nano-W or UF stain.

For 14 samples (d2.3 Fc, d2.4 Fc, d2.7 Fc, t32.4 Fc, t32.8 Fc, i52.6 Fc, d2.3 Fc, d2.4 IgG, d2.7 IgG, t32.4 IgG, t32.8 IgG, o42.1 IgG, i52.3 IgG and i52.6 IgG samples),



micrographs were recorded using Legikon software (52) on a 120 kV FEI Tecnai G2 Spirit with a Gatan Ultrascan 4000 4k × 4k CCD camera at 67,000 nominal magnification (pixel size 1.6 Å/pixel) or 52,000 nominal magnification (pixel size 2.07 Å) at a defocus range of 1.0 – 2.5 μm (Table S3).

5 For D3-08 Fc and D3-36 Fc samples, micrographs were recorded via manual acquisition on a 120 kV FEI L120C Talos TEM with a 4K × 4K Gatan OneView camera at 57,000 nominal magnification (pixel size 2.516 Å/pixel) at a defocus range of 1.0 – 2.5 μm.

#### 10 *NS-EM data analysis of Fc and IgG AbCs*

Particles were picked either with DoGPicker within the Appion interface (53) or cisTEM (54); both are reference-free pickers. Contrast-transfer function (CTF) was estimated using GCTF (55) or cisTEM. 2D class averages were generated in cryoSPARC (56) or in cisTEM. Reference-free *ab initio* 3D reconstruction using particles  
15 selected from 2D class averages from each dataset was performed in cryoSPARC or in cisTEM (Table S4).

#### *Cryo-EM specimen preparation and data collection of o42.1 and i52.3 AbCs*

3.0 μL of o42.1 Fc sample at 0.8 mg/mL in TBS pH 8.0 with 100mM Arginine was  
20 applied onto glow-discharged 1.2μm C-flat copper grids. 3.0 μL of i52.3 Fc sample at 0.1 mg/mL in TBS pH 8.0 was applied onto glow-discharged 1.2 μm C-flat copper grids coated with a thin layer of continuous homemade carbon. Grids were then plunge-frozen in liquid ethane, cooled with liquid nitrogen using an FEI MK4 Vitrobot with a 6

second blotting time and 0 force for o42.1 Fc, and 2.5 second blotting time and -1 force for i52.3 Fc. The blotting process took place inside the Vitrobot chamber at 20°C and 100% humidity. Data acquisition was performed with the Legimon data collection software on an FEI Glacios electron microscope at 200 kV and a Gatan K2 Summit camera. The nominal magnification was 36,000 with a pixel size of 1.16 Å/pixel. The dose rate was adjusted to 8 counts/pixel/s. Each movie was acquired in counting mode fractionated in 50 frames of 200 ms/frame.

#### *Cryo-EM data analysis of o42.1 and i52.3 AbCs*

10 For both o42.1 Fc and i52.3 Fc datasets, micrographs were motion-corrected using Warp (57) and exported to cryoSPARC for CTF estimation with CTFFIND4. A manually picked set of particles was used to generate 2D class averages that were subsequently used (after low-pass filtering to 20 Å resolution) for Template Picker in cryoSPARC on the whole dataset. Particles were extracted with a box size of 648 pixels and subjected to reference-free 2D classification in cryoSPARC.

15 For the o421.1Fc dataset, particles from selected 2D classes were classified using *ab initio* reconstruction in cryoSPARC with default parameters, 4 classes, and no symmetry imposed. Micrographs containing particles from 2 classes out of 4 resulting *ab initio* classes were subjected to Manually Curate Exposures function in cryoSPARC to remove bad micrographs. This set of particles after manual curation in cryoSPARC underwent another round of *ab initio* reconstruction in cryoSPARC with default parameters, 4 classes, and no symmetry imposed. One class (4032 particles) from these 4 resulting *ab initio* classes was selected for Non-uniform refinement (NUR) in

cryoSPARC with no symmetry applied or with O symmetry applied. The NUR map with no symmetry has a 17.7 Å resolution and the NUR map with O symmetry applied has a 11.14 Å resolution; both maps were similar, justifying imposing O symmetry for the final reconstruction.

5            For the i52.3 Fc dataset, after 1 round of 2D classification in cryoSPARC, the micrographs containing particles in a set of selected 2D classes were subjected to Manually Curate Exposures function in cryoSPARC to remove bad micrographs. This set of particles after manual curation in cryoSPARC were subjected to another round of 2D classification in cryoSPARC. 3,918 particles from selected 2D classes were  
10            reconstructed into one 3D class using *ab initio* reconstruction in cryoSPARC with no symmetry imposed, maximum and initial resolutions set to 6 Å and 12 Å respectively, initial and final minibatch sizes set to 1000 images. The resulting C1 *ab initio* map and particles then underwent NUR in cryoSPARC with no symmetry applied or with I  
15            symmetry applied. The NUR map with no symmetry has a 18.44 Å resolution and the NUR map with I symmetry applied has a 12.18 Å resolution; both maps were similar,  
20            justifying imposing I symmetry for the final reconstruction.

             All resolutions are reported based on the gold-standard Fourier shell correlation FSC (GSFSC) = 0.143 criterion (58, 59) and FSC curves were corrected for the effects of soft masking by high-resolution noise substitution (60). A summary of EM data  
20            acquisition and processing is provided in Tables S3-S4.

### **Computational design of AbCs concurrent with oligomer design**

Given the success in designing AbCs when using only previously-validated oligomers, we were curious whether we could design structures with newly-designed cyclic oligomers. This has the advantage of creating oligomer building blocks for future applications as well as additional antibody nanocages. First, C3s were generated by docking helical proteins into cyclic symmetries and designing a low-energy de novo interface (20). Those C3s were used to design 48 antibody nanocages across D3 dihedral (14), T32 tetrahedral (11), O32 octahedral (15), and I32 icosahedral (8) symmetries following the same fusion and design approach described above. From these designs, 36 were soluble, and two D3 dihedra (Fig. S5a) formed with Fc into structures very similar to the designed models according to SEC, SAXS, and NS-EM (Fig. S5b-e).

### **Stability experiments**

Samples were prepared for stability analysis by mixing equimolar amounts of each AbC-forming design component with hIgG1 Fc domain. These were purified using SEC using a Superose 6 column, following similar techniques as described above, into tris buffered saline (150 mM NaCl, 25 mM Tris-HCl pH 8.0) with 50 mM L-arginine (from a 1 M L-arginine pH 8.0); L-arginine was added to all designs as it had been observed to reduce hydrophobic association for the i52.6 AbCs. After SEC, the fractions corresponding to the AbC (left-most peak) were pooled. These were incubated at room temperature and analyzed once per week for up to five weeks post-SEC via DLS and SDS-PAGE. Designs d2.3 and d2.4 experiments were started three weeks later than the other six designs.

### *Dynamic light scattering*

Dynamic light scattering measurements (DLS) were performed using the default Sizing and Polydispersity method on the UNcle (Unchained Labs). 8.8  $\mu$ L of AbCs were pipetted into the provided glass cuvettes. DLS measurements were run in triplicate at 25°C with an incubation time of 1 second; results were averaged across runs and plotted using Graphpad Prism. Table S6 provides DLS summary data.

### *SDS-PAGE*

10 10  $\mu$ L of Fc AbCs were diluted to approximately 0.1 mg/mL and prepared for SDS by mixing with 2  $\mu$ L of 6 $\times$  loading dye (197 mM Tris-HCl, pH 6.8; 70% glycerol; 6.3% SDS; 0.03% bromophenol blue); these were then heated for 5-10 minutes at 95°C and loaded into the wells of a Tris-Glycine gel (Bio-Rad, catalogue #5678125). SDS running buffer was prepared to a final concentration of 5 mM Tris, 192 mM glycine, 15 0.1% SDS, pH 8.3. 2-5  $\mu$ L of ladder was also added (BioRad 161-0377 or 161-0374). The gel was run for 25-30 minutes at 180-200 V or until the dye reached near the bottom of the gel. Gels were stained with Coomassie Brilliant Blue dye using the Genscript eStain protein staining system.

### *Exchange experiments*

GFP-Fc and RFP-Fc were produced in Expi293F cells and purified as described above. GFP-Fc was mixed with o42.1 tetramer; a pre-mixed ratio of RFP-Fc and GFP-Fc (at a 25:1 molar ratio) was separately combined with o42.1 tetramer as a positive

control meant to mimic 100% exchange (as the GFP-Fc o42.1 AbC would be mixed with 25-fold excess RFP-Fc). Fc-GFP o42.1 and 25:1 Fc-RFP:GFP o42.1 were purified via a Superose 6 SEC column into TBS (150 mM NaCl, 25 mM Tris-HCl pH 8.0) with 50 mM L-arginine. Fc-GFP o42.1 was then incubated with 25-fold excess Fc-RFP at a final  
5 volume of 2 mL and separated using an autosampler set to inject 470  $\mu$ L; the autosampler was necessary to control injection volume (Cytiva ALIAS autosampler). Time points were taken at 5 minutes, 2 hours, 4 hours, and 24 hours after mixing and incubation at 25°C. Controls were GFP-Fc o42.1 without added Fc-RFP, Fc-RFP without AbC, and the “pre-exchanged” control normalized to the GFP-Fc o42.1 molarity.  
10 100  $\mu$ L from each peak fraction were then added to a 96-well fluorescence plate (Corning, black polystyrene). To measure GFP signal, excitation and emission wavelengths were set to 485/510 (respectively); for RFP signal, excitation and emission wavelengths were set to 558/605; fluorescence readings were taken with the Neo2 Microplate Reader (BioTek).

15

## **DR5 and A1F-Fc experiments**

### *Cell culture*

Colorectal adenocarcinoma cell line-Colo205, and renal cell carcinoma cell line RCC4 were obtained from ATCC. Primary kidney tubular epithelial cells RAM009 were  
20 a gift from Dr. Akilesh (University of Washington). Colo205 cells were grown in RPMI1640 medium with 10% Fetal Bovine Serum (FBS) and penicillin/streptomycin. RCC4 cells were grown in Dulbecco’s Modified Eagle’s Medium with 10% FBS and penicillin/streptomycin. RAM009 were grown in RPMI with 10% FBS, ITS-supplement,

penicillin/streptomycin and Non Essential Amino Acids (NEAA). All cell lines were maintained at 37°C in a humidified atmosphere containing 5% CO<sub>2</sub>.

Human Umbilical Vein Endothelial Cells (HUVECs, Lonza, Germany, catalog # C2519AS) were grown on 0.1% gelatin-coated 35 mm cell culture dish in EGM2 media.

5 Briefly, EGM2 consist of 20% Fetal Bovine Serum, 1% penicillin-streptomycin, 1% Glutamax (Gibco, catalog #35050061), 1% endothelial cell growth factor (32), 1mM sodium pyruvate, 7.5mM HEPES, 0.08mg/mL heparin, 0.01% amphotericin B, a mixture of 1× RPMI 1640 with and without glucose to reach 5.6 mM glucose concentration in the final volume. Media was filtered through a 0.45-µm filter. HUVECs at passage 7 were  
10 utilized in Tie2 signaling experiments. HUVECs at passage 6 were used in the tube formation assay.

#### *Caspase-Glo 3/7 and Caspase-Glo 8 assays*

Cells were passaged using trypsin and 40,000 cells/well were plated onto a 96-  
15 well white tissue culture plate and grown in appropriate media. Medium was changed the next day (100 µL/well) and cells were treated with either uncaged α-DR5 AMG655 antibody (150nM), recombinant human TNF Related Apoptosis Inducing Ligand (TRAIL; 150nM), Fc-only AbCs or α-DR5 AbCs (150nM, 1.5nM, 15pM for caspase-3/7; only 150 nM and 1.5 nM were tested for caspase-8) and incubated at 37°C for 24 hours  
20 (caspase-3/7) or 12 hours (caspase-8). In all cases here and throughout, the antibody or AbC concentration refers to the protein's asymmetric unit (e.g, the molar unit for the antibody is 1 heavy chain and 1 light chain). The following day, 100 µL/well of Caspase-Glo 3/7 reagent or Caspase-Glo 8 reagent (Promega, USA) was added into the media

and incubated for 1 hour (caspase-3/7) or 2 hours (caspase-8) at 37°C. Luminescence was then recorded using Perkin EnVision microplate reader (Perkin Elmer). Statistical comparisons were performed using Graphpad Prism (see Table S8 for full detail).

#### 5 *Titer Glo cell viability assay (4 d viability)*

Cells were plated onto a 96-well plate at 20,000 cells/well. The next day, cells were treated with 150nM of  $\alpha$ -DR5 AbCs, TRAIL and  $\alpha$ -DR5 antibody for 4 d. At day 4, 100  $\mu$ L of CellTiter-Glo reagent (Promega Corp. USA, #G7570) was added to the 100  $\mu$ L of media per well, incubated for 10 min at 37°C and luminescence was measured using a Perkin-Elmer Envision plate reader.

#### *Alamar Blue cell viability assay (6 d viability)*

Cells were seeded onto a 12-well tissue culture plate at 50,000 cells/well. The next day, cells were treated with  $\alpha$ -DR5 AbCs, TRAIL, or  $\alpha$ -DR5 antibodies at 150 nM concentration. Three days later cells were passaged at 30,000 cells/well and treated with 150 nM of  $\alpha$ -DR5 cages, TRAIL and  $\alpha$ -DR5 antibody for 3 days. At 6 days, the media was replaced with 450  $\mu$ L/well of fresh media and 50  $\mu$ L of Alamar blue reagent (Thermofisher Scientific, USA, #DAL1025) was then added. After 4 hours of incubation at 37°C, 50  $\mu$ L of media were transferred into a 96-well opaque white plate and fluorescence intensity was measured using plate reader according to manufacturer's instructions.

#### *Protein isolation for western blot analysis*



Cells were passaged onto a 12-well plate at 80,000 cells/well and were grown until 80% confluency is reached. Before treatment the media was replaced with 500  $\mu$ L of fresh media. For DR5 experiments, AMG-655 antibody and TRAIL were added at 150 nM concentration and Fc-only nanocages or  $\alpha$ -DR5 nanocages were added at 150 nM, 5 1.5 nM and 15  $\mu$ M concentration onto the media and incubated for 24 hours at 37°C prior protein isolation; as above, concentrations are calculated based on the asymmetric unit. For the caspase inhibition experiment, RCC4 cells were pre-treated for 30 minutes with 10  $\mu$ M of zVAD followed by treatment with 150nM o42.1  $\alpha$ -DR5 Ab for additional 24 hours, and total protein isolation.

10 Media containing dead cells was transferred to a 1.5 mL Eppendorf tube, and the cells were gently rinsed with 1 $\times$  phosphate buffered saline. 1 $\times$  trypsin was added to the cells for 3 minutes. All the cells were collected into the 1.5 mL Eppendorf containing the medium with dead cells. Cells were washed once in PBS 1 $\times$  and lysed with 70  $\mu$ L of lysis buffer containing 20 mM Tris-HCl (pH 7.5), 150 mM NaCl, 15% Glycerol, 1% 15 Triton, 3% SDS, 25 mM  $\beta$ -glycerophosphate, 50mM NaF, 10mM Sodium Pyrophosphate, 0.5% Orthovanadate, 1% PMSF (all chemicals were from Sigma-Aldrich, St. Louis, MO), 25 U Benzonase Nuclease (EMD Chemicals, Gibbstown, NJ), protease inhibitor cocktail (Pierce™ Protease Inhibitor Mini Tablets, Thermo Scientific, USA), and phosphatase inhibitor cocktail 2 (catalog#P5726), in their respective tubes). 20 Total protein samples were then treated with 1  $\mu$ L of Benzonase (Novagen, USA) and incubated at 37°C for 10 minutes. 21.6  $\mu$ L of 4x Laemmli Sample buffer (Bio-Rad, USA) containing 10% beta-mercaptoethanol was added to the cell lysate and then heated at 95°C for 10 minutes. The boiled samples were either used for western blot analysis or

stored at -80 °C.

### *Western blotting*

The protein samples were thawed and heated at 95°C for 10 minutes. 10 µL of protein sample per well was loaded and separated on a 4-10% SDS-PAGE gel for 30 minutes at 250 V. The proteins were then transferred onto a Nitrocellulose membrane for 12 minutes using the semi-dry turbo transfer western blot apparatus (Bio-Rad, USA). Post-transfer, the membrane was blocked in 5% nonfat dry milk for 1 hour. After 1 hour, the membrane was probed with the respective antibodies: cleaved-PARP (Cell Signaling #9541, USA) at 1:2000 dilution; Cleaved-caspase 8 (Cell signaling #9496, USA) at 1:2000 dilution; pERK1/2 (Cell Signaling) at 1:5000 dilution; pFAK (Cell Signaling) at 1:1000 dilution; p-AKT(S473) (Cell Signaling) at 1:2000 dilution; and actin (Cell Signaling, USA) at 1:10,000 dilution. Separately, for p-AKT(S473) the membrane was blocked in 5% BSA for 3 hours followed by primary antibody addition. Membranes with primary antibodies were incubated on a rocker at 4°C, overnight. Next day, the membranes were washed with 1× TBST (3 times, 10 minutes interval) and the respective HRP-conjugated secondary antibody (Bio-Rad, USA) (1:10,000) was added and incubated at RT for 1 hour. For p-AKT(S473), following washes, the membrane was blocked in 5% milk at room temperature for 1 hour and then incubated in the respective HRP-conjugated secondary antibody (1:2000) prepared in 5% milk for 2 hours. After secondary antibody incubation, all the membranes were washed with 1× TBST (3 times, 10 minutes interval). Western blots were developed using Luminol reagent (Immobilon Western Chemiluminescent HRP Substrate, Millipore) for 3-15 seconds and imaged

using Bio-Rad ChemiDoc Imager. Data were quantified using the ImageJ software to analyze band intensity.

Quantifications were done by calculating the peak area for each band. Each signal was normalized to the actin quantification from that lane of the same gel, to allow  
5 for cross-gel comparisons. Fold-changes were then calculated compared to PBS for all samples except for the pAKT reported for the A1F-Fc western blot (there was not enough pAKT signal for comparison, so o42.1 A1F-Fc was used for normalization). Statistical comparisons were performed using Graphpad Prism (see Tables S8, S9 for full detail). For all statistical analyses, means were compared to the PBS condition.

10

#### *Tube formation assay (vascular stability)*

Vascular stability and tube formation were assessed using a protocol modified from a previous report (61). Briefly, passage 6 HUVECs were seeded onto 24-well plates precoated with 150  $\mu$ L of 100% cold Matrigel (Corning, USA) at 150,000  
15 cells/well density, along with scaffolds at 89 nM F-domain concentrations or PBS in low glucose DMEM medium supplemented with 0.5% FBS for 24 hours. At the 24 hour time point, old media was aspirated and replaced with fresh media without added AbCs or controls. The cells were incubated up to 72 hours. Cells were imaged at 48 hour and 72 hour time points using Leica Microscope at 10 $\times$  magnification under phase contrast.  
20 Thereafter, the tubular formations were quantified by calculating the number of nodes, meshes and tubes using the Angiogenesis Analyzer plugin in Image J software. Vascular stability was calculated by averaging the number of nodes, meshes, and tubes, and then normalizing to PBS. Statistical comparisons were performed using

Graphpad Prism (see Table S9 for full detail).

*Human serum A1F-Fc AbC incubation experiment*

HUVECs (C2519AS, Lonza) were grown to at least 80% confluence in 24-well  
5 plate format pre-treated with attachment factor (S006100, ThermoFisher) and cultured  
in EGM-2 growth medium (CC-3162, Lonza) according to manufacturer's instructions.  
The cells were then starved in DMEM low glucose serum-free media (11885084, Gibco)  
for 24 hrs. In parallel, proteins were incubated in 100% human serum (Sigma, H4522-  
100ML) at 1.5  $\mu$ M for 24 hours at 4°C or 37°C; dilutions of AbC into serum were  
10 approximately 1:4 (AbC to final, v/v). After starvation and protein incubation, cell media  
was replaced, and proteins were added to the cells at a final concentration of 150 nM  
for 30 minutes at 37°C. Conditions with human serum were all normalized to a final  
concentration of 10% upon addition to the cell media. After treatment, the media was  
aspirated and cells were washed once with PBS before lysis. Cells were lysed with 60  
15  $\mu$ L of lysis buffer containing 50 mM HEPES, 150 mM NaCl, 10% Glycerol, 1% Triton X-  
100, 3% SDS, 25 mM  $\beta$ -glycerophosphate, 100 mM NaF, 10 mM Sodium  
Pyrophosphate, 1 mM EGTA, 1.5 mM MgCl<sub>2</sub>, 1% Sodium Orthovanadate, 300  $\mu$ M  
PMSF, 25 U DNase, 1% phosphatase inhibitor cocktail 2 (all chemicals were from  
Sigma-Aldrich), and protease inhibitor cocktail (Pierce™ Protease Inhibitor Mini  
20 Tablets, Thermo Scientific, USA). Cell lysate was collected in a fresh Eppendorf tube.  
Lysate samples were prepared using the Anti-Rabbit Detection Module for the Jess  
instrument (ProteinSimple) and boiled for 10 minutes at 98°C. A 12-230 kDa 25-  
capillary cartridge and microplate were utilized for the Jess instrument, using the anti-

phospho-Akt (S473) (D9E) XP rabbit mAb (4060, Cell Signaling) with a 30 minute incubation time. Replicate chemiluminescent peak values corresponding to phospho-Akt (~56 kDa) are reported.

## 5 Immune cell activation materials and methods

### *CD40 luminescence assay*

A non-agonistic antibody (clone LOB7/6, product code MCA1590T, BioRad), was combined with the octahedral o42.1 AbC-forming design as described above and further characterized by DLS and NS-EM (Fig. S10). Negative control o42.1 AbC was made using a non-CD40 binding IgG (mpe8), which binds to RSV spike protein (44). These two AbCs, along with uncaged LOB7/6 and a positive control CD40-activating IgG (Promega, catalog #K118A) were diluted to make a 10-point, threefold dilution series for triplicate technical repeats starting at 1.2  $\mu$ M; as described above, concentrations are calculated based on the asymmetric unit. The positive control CD40-activating IgG (K118A) is a murine IgG1a antibody, it was not compatible for assembly with the o42.1 design, likely due to the low binding interface between protein A and mIgG1a (data not shown). Particles were filtered using a 0.22  $\mu$ m syringe filter (Millipore) and AbC formation was assessed using SEC and DLS using procedures described above. SEC was used as an analytical technique to show absence of unassembled components; due to the expense of commercial antibodies and the typical loss of yield using SEC as would be expected for any filtration technique, we did not use SEC as a separation technique here prior to DLS measurements or in vitro assays. SEC and DLS confirm the presence of the designed assemblies and absence of off-target or unassembled

species; the o42.1 AbCs eluted in the SEC void of the Superose 6 column as expected given their designed and verified radii (~40 nm when formed with IgGs). Post-filtration concentration readings were taken and confirmed that there was no sample loss when using the syringe filter.

5           To assay CD40 activation, we followed manufacturer's instructions for a bioluminescent cell-based assay that measures the potency of CD40 response to external stimuli such as IgGs (Promega, JA2151). Briefly, CD40 effector Chinese Hamster Ovary (CHO) cells were cultured and reagents were prepared according to the assay protocol. The antibodies and AbCs were incubated with the CD40 effector CHO  
10 cells for 8 hours at 37°C, 5% CO<sub>2</sub>. Bio-Glo™ Luciferase Assay System (G7941) included in the assay kit is used to visualize the activation of CD40 from luminescence readout from a plate reader. The Bio-Glo™ Reagent is applied to the cells and luminescence was detected by a Synergy Neo2 plate reader every min for 30 minutes. Data were analyzed by averaging luminescence between replicates and subtracting  
15 plate background. The fold induction of CD40-binding response was determined by RLU of sample normalized to RLU of no antibody controls. Data curves were plotted and EC50 was calculated using GraphPad Prism using the log(agonist) vs. response -- Variable slope (four parameters); see Table S10 for EC50 values and 95% CI values.

20

#### *T cell proliferation and flow cytometry*

Mosaic AbCs were formed by mixing  $\alpha$ -CD3 (clone name: OKT3, BioLegend) and  $\alpha$ -CD28 (CD28.6, catalog #16-0288-85, ThermoFisher) antibodies together first, and

then combining with excess o42.1 AbC-forming design. Mosaic  $\alpha$ -CD3/28 o42.1 cages were purified via SEC into PBS as described above. SEC and DLS confirmed the assembly of o42.1 AbCs, which eluted as expected into the void volume in SEC given the particle's size.

5 Primary human peripheral blood mononuclear cells (PBMC) were obtained upon written informed consent from the Virginia Mason Medical Center in Seattle, WA, USA. All studies were approved by the Institutional Review Board of the Benaroya Research Institute (Seattle, WA). Naive CD4<sup>+</sup> conventional human T cells (CCR7<sup>+</sup>CD45RA<sup>+</sup>CD127<sup>hi</sup>CD25<sup>neg</sup>) were isolated from PBMC by cell sorting to >99%  
10 purity. PBMC were first labeled with 2.5  $\mu$ M Cell Proliferation Dye e670 (ThermoFisher) according to manufacturer instructions, then rested for 1h at 37C 5% CO<sub>2</sub>. CPD-labeled cells were harvested, incubated with viability dye ef780 (ThermoFisher) and stained in buffer containing HBBS + 0.3% BSA with indicated fluorescently labeled surface markers. Cell sorting and analysis were performed on a FACSAria Fusion (BD  
15 Biosciences) using an 85  $\mu$ M nozzle at 45 psi. Sorted T cells (1e6/mL) were incubated in the presence of indicated stimulation conditions (0.01 $\mu$ M) in ImmunoCult-XF T Cell Expansion Medium (Stem Cell). After 4-5 days, cells were harvested and re-stained with fluorescent antibodies. Data were analyzed using FlowJo software (Tree Star, Inc.)

## 20 **Viral neutralization**

*CV1, CV3, CV30*

$\alpha$ -CoV-2 S cages using CV IgGs were prepared by mixing  $\alpha$ -CoV-2 S IgGs with a 1:1 molar ratio of o42.1 design component and purifying via SEC into TBS, following similar protocols to those as described above for AbC assembly.

HIV-1 derived viral particles were pseudotyped with full length wildtype SARS  
5 CoV-2 S (62). Briefly, plasmids expressing the HIV-1 Gag and pol (pHDM-Hgpm2, BEI resources Cat# NR-52517), HIV-1Rev (pRC-CMV-rev1b, BEI resources Cat# NR-52519), HIV-1 Tat (pHDM-tat1b, BEI resources Cat# NR-52518), the SARS CoV2 spike (pHDM-SARS-CoV-2 Spike, BEI resources Cat# NR-52514) and a luciferase/GFP reporter (pHAGE-CMV-Luc2-IRES-ZsGreen-W, BEI resources Cat# NR-52516) were  
10 co-transfected into 293T cells at a 1:1:1:1.6:4.6 ratio using 293 Free transfection reagent (EMD Millipore Cat# 72181) according to the manufacturer's instructions. Transfected cells were incubated at 32°C for 72 hours after which the culture supernatant was harvested, clarified by centrifugation and frozen at -80°C.

293 cells stably expressing ACE2 (HEK-293T-hACE2, BEI resources Cat# NR-  
15 5251) were seeded at a density of  $4 \times 10^3$  cells/well in a 100  $\mu$ L volume in 96 well flat bottom clear bottomed, black walled plates (Greiner Bio-One Cat # 655090) (62). The next day, IgG alone, or in complex with cage components were serially diluted in 30 $\mu$ L of cDMEM in 96 well round bottom plates in triplicate; as described above, concentrations are calculated based on the asymmetric unit.

20 An equal volume of viral supernatant was added to each well and incubated for 60 min at 37°C. Meanwhile 50  $\mu$ L of cDMEM containing 6 $\mu$ g/ml polybrene was added to each well of 293T-ACE2 cells (2 $\mu$ g/ml final concentration) and incubated for 30 min. The media was aspirated from 293T-ACE2 cells and 100 $\mu$ L of the virus-antibody mixture was



added. The plates were incubated at 37°C for 72 hours. The supernatant was aspirated and replaced with 100 µL of Steadyglo luciferase reagent (Promega) and the plate was read on a Fluorskan Ascent Fluorimeter. Control wells containing virus but no antibody (cells + virus) and no virus or antibody (cells only) were included on each plate.

5           Percent neutralization for each well was calculated as the RLU of the average of the cells + virus wells, minus test wells (cells + mAb + virus), and dividing this result difference by the average RLU between virus control (cells + virus) and average RLU between wells containing cells alone, multiplied by 100. The antibody concentration that neutralized 50% of infectivity (IC50) was interpolated from the neutralization curves  
10           determined using the log(inhibitor) vs. response -- Variable slope (four parameters) fit using Graphpad Prism Software. Experiments were performed in duplicate. See Table S4 for IC50 values and 95% CI values.

### *Fc-ACE2*

15           Murine leukemia virus (MLV)-based SARS-CoV-2 S-pseudotyped viruses were prepared as previously described (43). Briefly, HEK293T cells were co-transfected with a SARS-CoV-2 S encoding-plasmid, an MLV Gag-Pol packaging plasmid and the MLV transfer vector encoding a luciferase reporter using the Lipofectamine 2000 transfection reagent (Life Technologies) according to the manufacturer's protocols. Transfection  
20           mixture was added dropwise to HEK293T cells. Cells were then incubated in the transfection mixture and OPTI-MEM for 5 hours at 37°C with 8% CO<sub>2</sub> before the medium was exchanged into DMEM containing 10% FBS. After 72 hours, the pseudovirus-containing supernatant was collected, centrifuged for 10 minutes at 3000×g

to clear cell debris and filtered using a 0.45um filter with PES-membrane (MilliporeSigma). The pseudoviruses were concentrated using 30 kDa cut-off concentrators (Amicon) and stored at -80°C until further use.

HEK-293T-hACE2 (BEI resources Cat# NR-5251) were cultured in DMEM containing 10% FBS and 1% PenStrep (62). 16-24 hours before infection, cells were plated into white sided clear bottom 96-well plates coated with Poly-L-Lysine solution (Sigma Aldrich, Cat #: P4707). Briefly, 25 µL Poly-L-Lysine solution was added to each well. The plate was incubated at RT for 10 minutes before removal of Poly-L-Lysine and washing with tissue culture grade water. The Poly-L-lysine coated plate was dried for 10 minutes before the cell plating step. Prior to transfection the HEK-293T-hACE2 96 well plates were washed 3 times with DMEM. Fc-ACE2 (Sinobiologicals, Cat #: 10108-H02H), o42.1 Fc, and o42.1 Fc-ACE2 were purified via SEC as described above, and serially diluted 2× in DMEM starting from 800nM; all concentrations are calculated based on the asymmetric unit. Equal volumes of concentrated pseudovirus and serial dilution of treatments (Fc-ACE2, o42.1 Fc particles or o42.1 Fc-ACE2 particles or DMEM) were combined and incubated for 30 minutes and then added to the cells. After 2-3 hours, DMEM containing 20% FBS and 2% PenStrep was added to the cells. 48 hours post infection, One-Glo-EX (Promega) was added to the cells and incubated in the dark for 5-10 minutes prior to reading on a Varioskan LUX plate reader (ThermoFisher). As above, the antibody concentration that neutralized 50% of infectivity (IC50) was interpolated from the neutralization curves determined using the log(inhibitor) vs. response -- Variable slope (four parameters) using Graphpad Prism Software. The difference in IC50 was compared using the extra sum-of-squares F-test

function in Prism with a P-value cutoff at 0.05. Experiments were performed in technical duplicate. See Table S11 for IC50 values and 95% CI values.

5

10

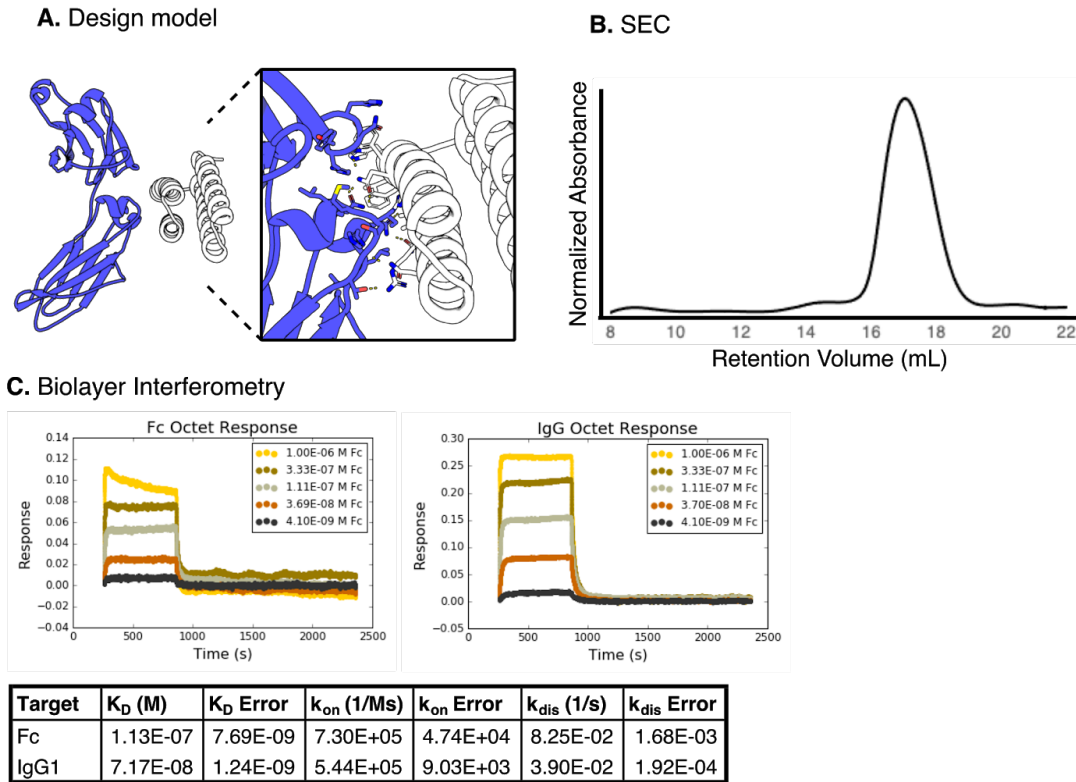


**Figure S1. Designed Fc-binding designed helical repeat.** **A**, Model of the helical repeat protein DHR79 docked against antibody Fc (PDB ID: 1DEE). Residues from protein A (PDB ID: 1L6X) are grafted at the interface between the Fc and the helical repeat protein. **B**, SEC trace of the Fc-binding helical repeat monomer. **C**, Biolayer interferometry (BLI) of the Fc-binding helical repeat design with Fc (left) or with hIgG1 (right), with summary statistics (below).

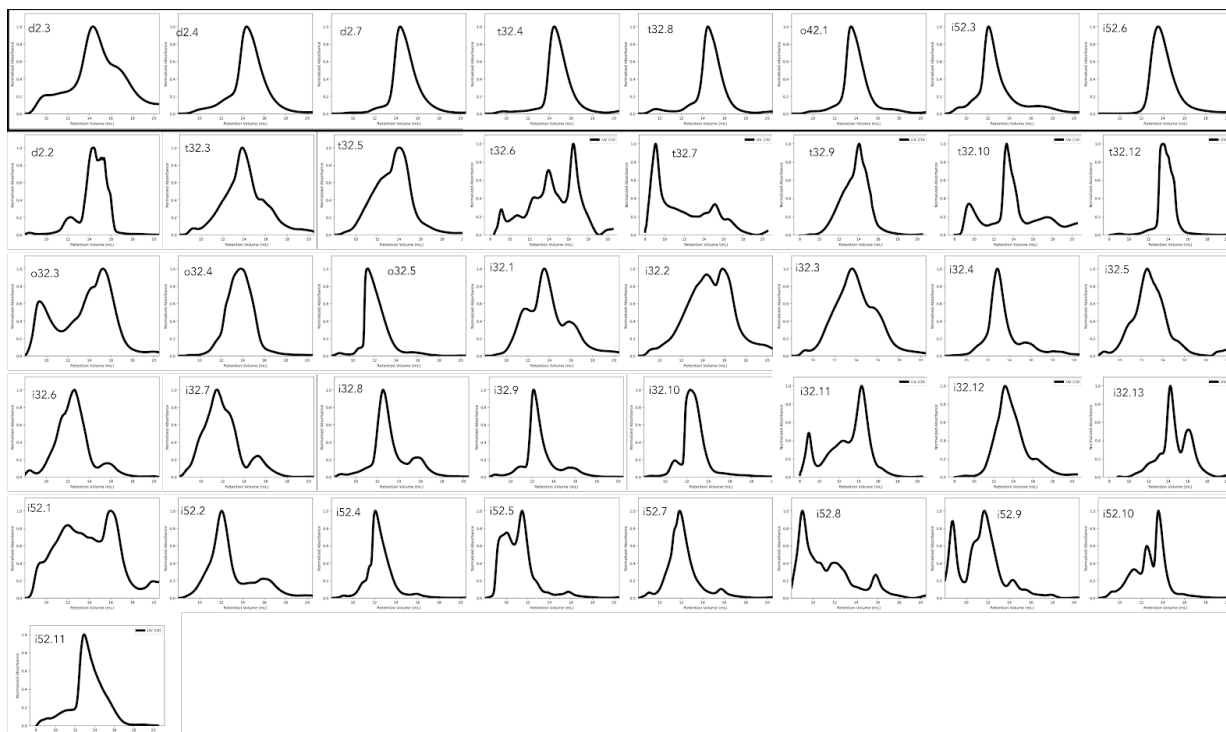
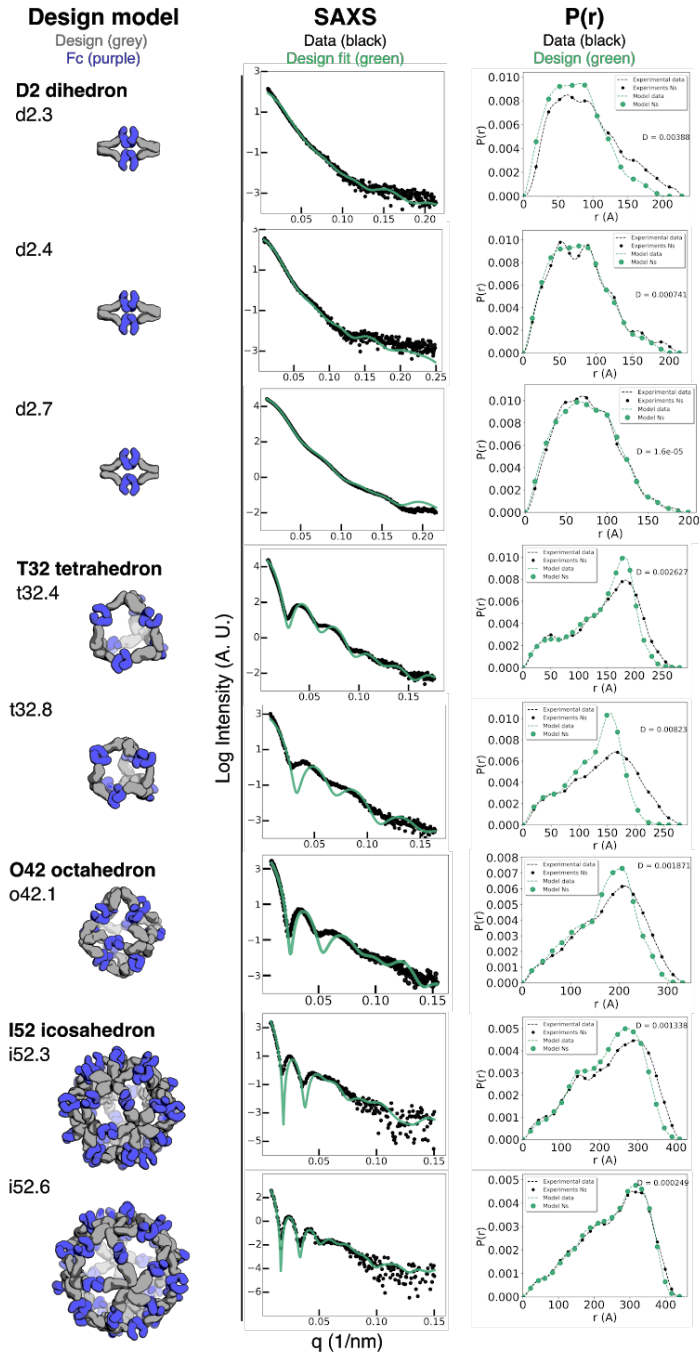


**Figure S2. SEC profiles for all soluble designs.** First row: SEC profiles of all soluble antibody nanocage-forming designs run over a Superose S200 column. Bottom rows: all other designs that did not form nanocages when mixed with antibodies. Several designs appear to still form oligomers at the expected size, but these may not have formed at the right orientation to lead to successful nanocage formation. X-axis for each is retention volume, and the Y-axis is normalized A230 absorbance.

5

10

15



5 **Figure S3. SAXS profiles for AbCs formed with Fc.** Left: design models show designed Fc-binding oligomers in grey and antibody Fc in purple. Middle: small angle X-ray scattering (SAXS) curve fit for all designs with Fc; Black dots represent experimentally-determined data, and the green lines are calculated from the design models, with the FOXS server (18) used to perform the curve fitting. Right: Distance distribution functions ( $P(r)$  curves) for experimental data (black) compared to theoretical distribution functions from the design models (green); Scatter3 was used to perform the  $P(r)$  analyses.

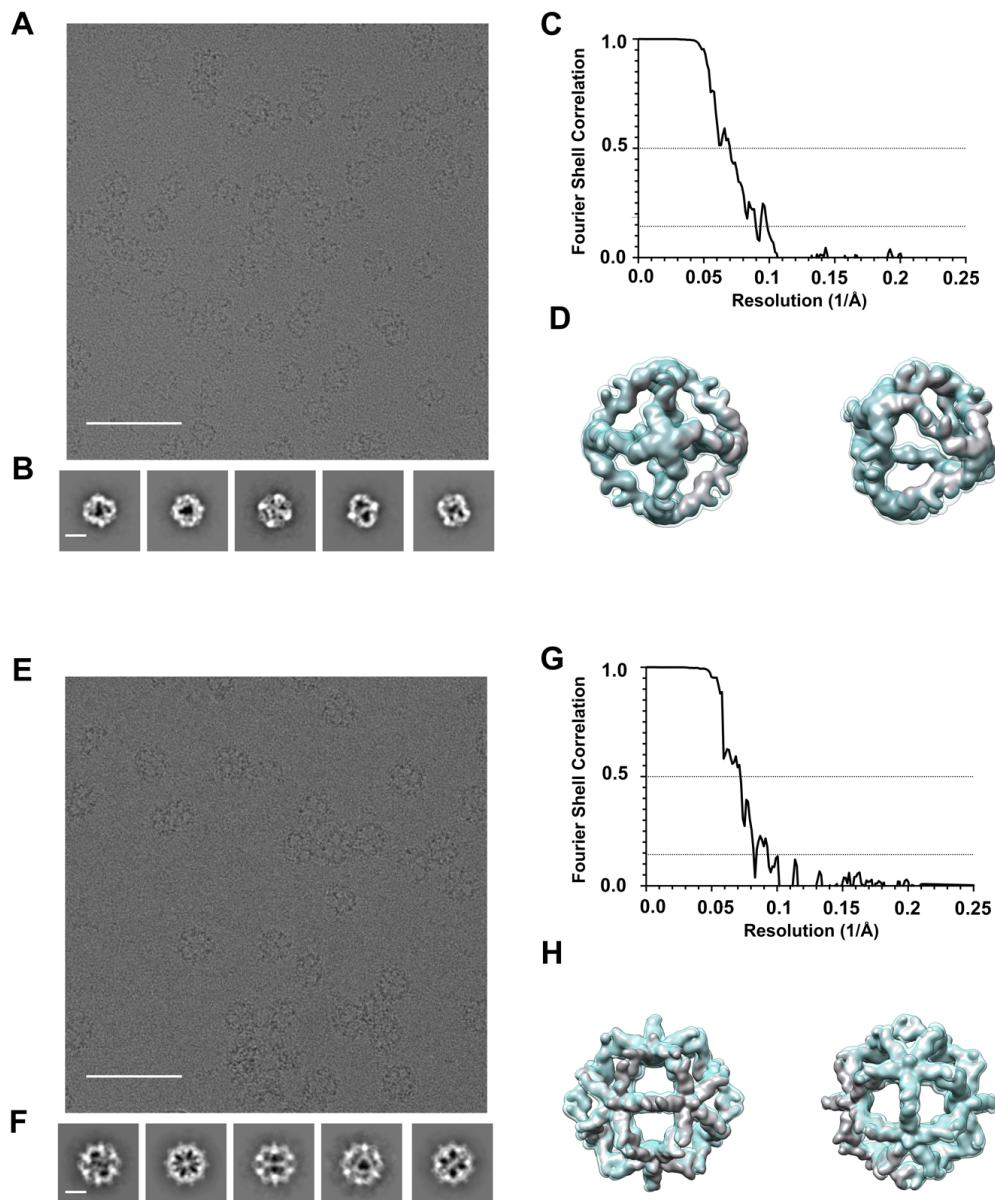


**Figure S4. Cryo-EM characterization of o42.1 Fc (A-D) and i52.3 Fc AbCs (E-H).** **A**, Representative cryo EM micrograph of o42.1 Fc. Scale bar: 100Å. **B**, Reference-free 2D class averages of o42.1-Fc. Scale bar, 200 Å. **C**, Gold-standard Fourier shell correlation curves for the o42.1 Fc map with O symmetry applied. Dotted line indicates the 0.143 and 0.5 thresholds. **D**, Two views of the o42.1 Fc cryo-EM map reconstructed with no symmetry (transparent cyan) superimposed on the o42.1 Fc cryo-EM map with O symmetry applied (solid gray). **E**, Representative micrograph of i52.3 Fc. Scale bar: 100Å. **F**, Reference-free 2D class averages of i52.3 Fc. Scale bar, 200 Å. **G**, Gold-standard Fourier shell correlation curves for the i52.3 Fc map with I symmetry applied. Dotted line indicates the 0.143 and 0.5 thresholds. **H**, Two views of the i52.3 Fc cryo-EM map reconstructed with no symmetry (transparent cyan) superimposed on the i52.3 Fc cryo-EM map with I symmetry applied (solid gray).

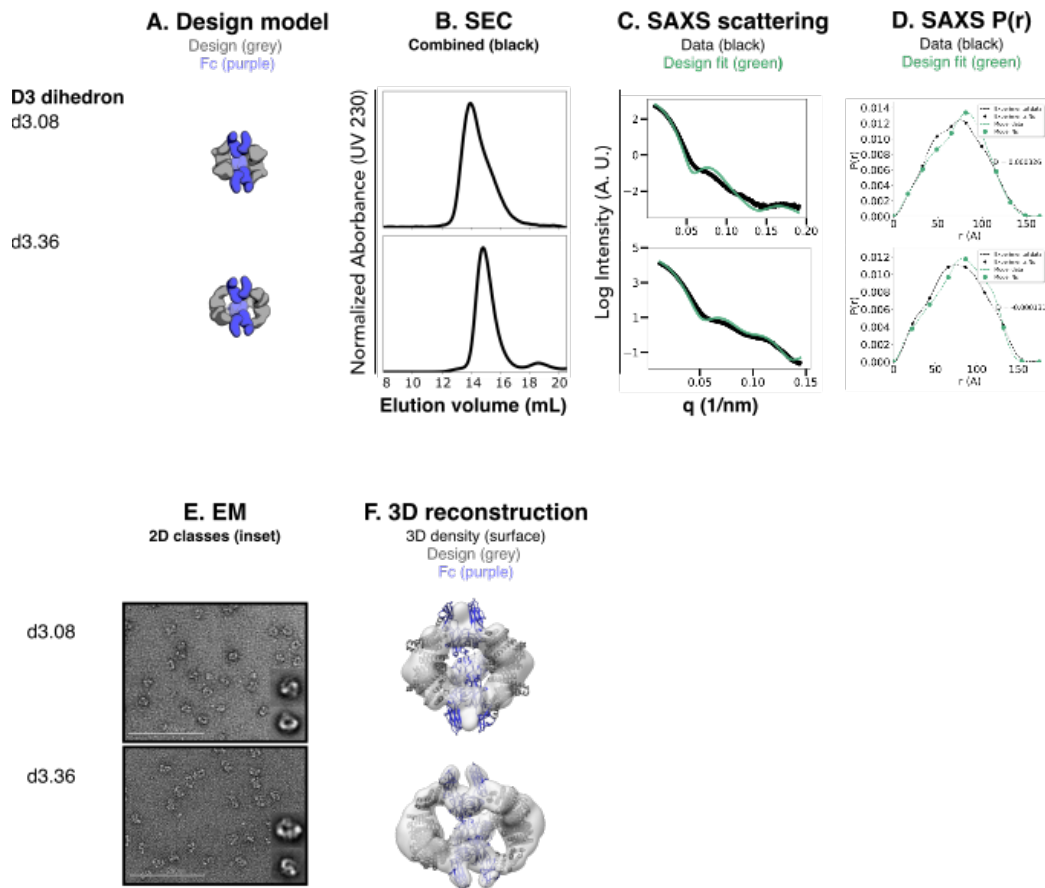


**Figure S5. Structural characterization of D3 dihedral AbCs with newly designed oligomers.** **A**, Design models, with antibody Fc (purple) and designed particle-forming oligomers (grey). **B**, SEC of the assembled AbC with Fc. **C**, SAXS curve fits for all designs with Fc; Black dots represent experimentally-determined data, and the green lines are calculated from the design models, with the FOXS server (18) used to perform the curve fitting. **D**, Distance distribution functions (P(r) curves) for experimental data (black) compared to theoretical distribution functions from the design models (green); Scatter3 was used to perform the P(r) analyses (reference). **E**, EM images with 2D averages in inset. **F**, 3D reconstructions from NS-EM data.

15

20



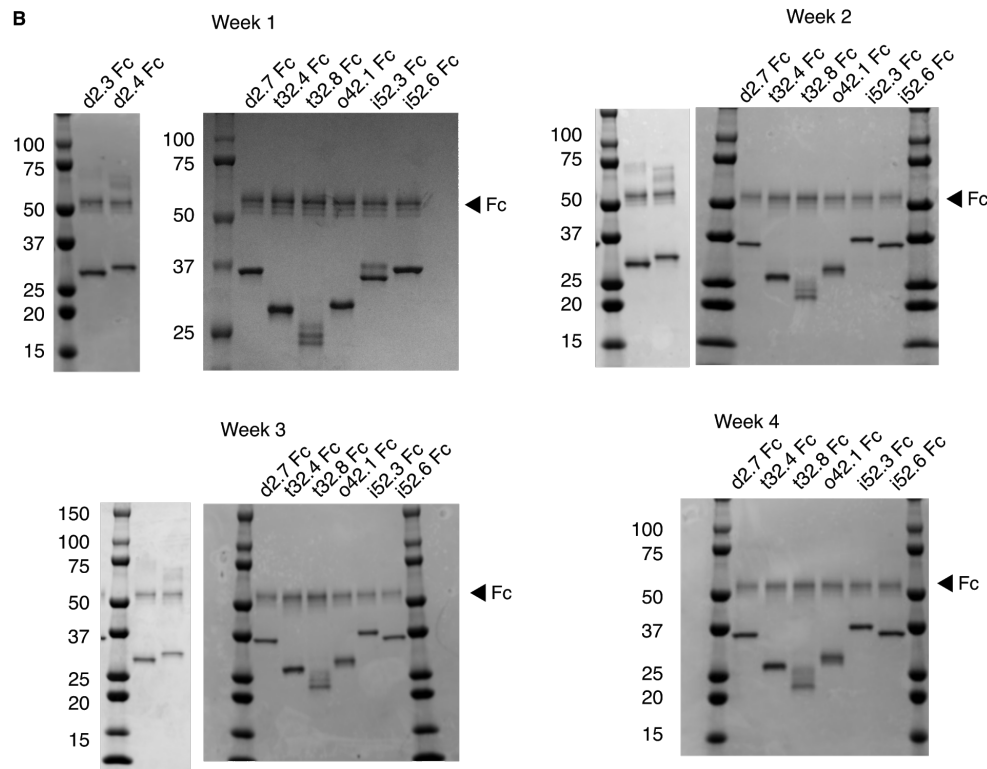
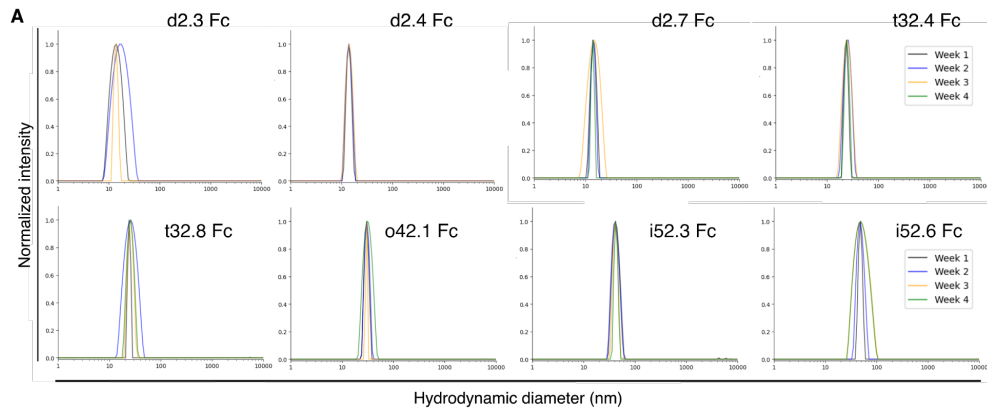


**Figure S6. Fc AbC particle stability over time.** **A**, Dynamic light scattering (DLS) of Fc AbCs, incubated at 25°C, and measured once per week. Traces are an average of 4 measurements each. **B**, SDS-PAGE analysis of Fc AbCs (without reducing agent), incubated at 25°C, and measured once per week. Molecular mass standards were run on outer lanes with masses (KDa) labeled.

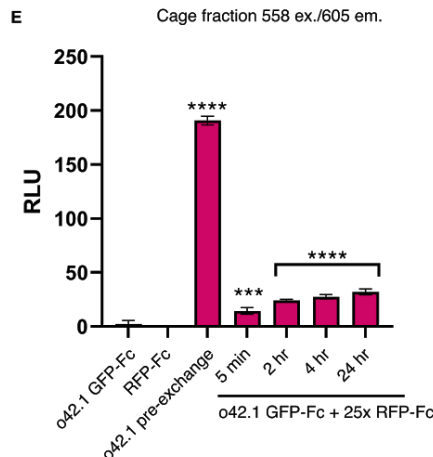
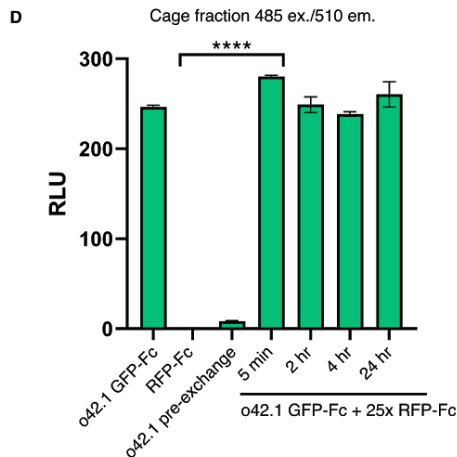
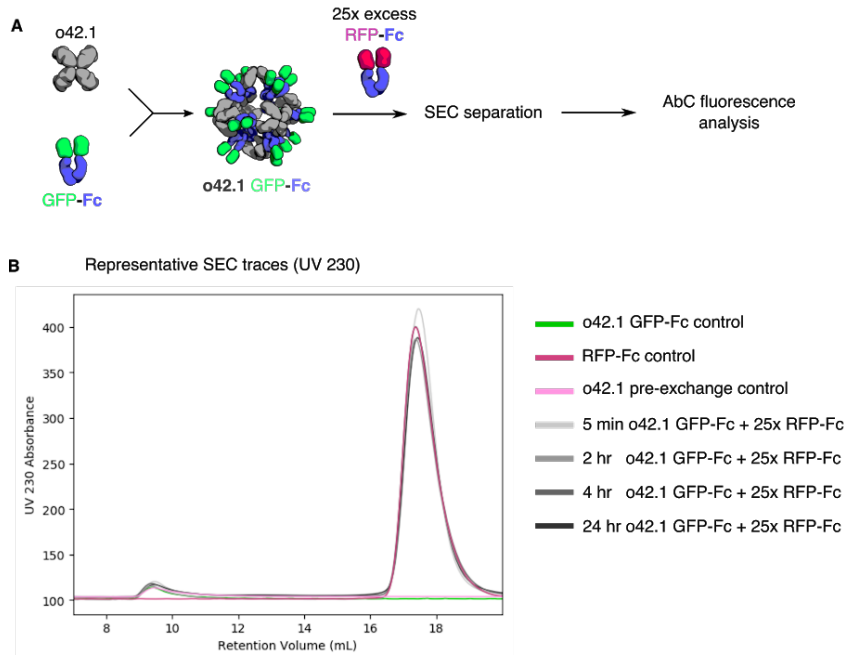


**Figure S7. o42.1 AbC formed with GFP-Fc minimally exchanges with free 25-fold excess RFP-Fc.** **A**, o42.1 AbCs are formed with GFP-Fc, purified, and incubated with 25-fold molar excess of RFP-Fc for up to 24 hours at room temperature. SEC is used to purify cage away from excess Fc-fusion; if AbCs exchange with free Fc-fusions, GFP signal would decrease in the cage fraction as RFP signal increases. Controls include: o42.1 GFP-Fc alone; RFP-Fc alone; and “pre-exchanged” o42.1 AbC prepared by pre-mixing RFP-Fc and GFP-Fc at a 25:1 molar ratio prior to AbC formation. **B**, representative SEC traces showing UV 230 absorbance. **C**, GFP signal briefly increases in the cage fraction for the o42.1 GFP-Fc AbCs incubated with 25-fold excess RFP-Fc, but drops to control o42.1 GFP-Fc levels, which is maintained for 24 hours at room temperature. **D**, RFP signal is increased in the cage fraction of o42.1 GFP-Fc AbCs incubated with Fc-RFP by less than 20% over 24 hours.

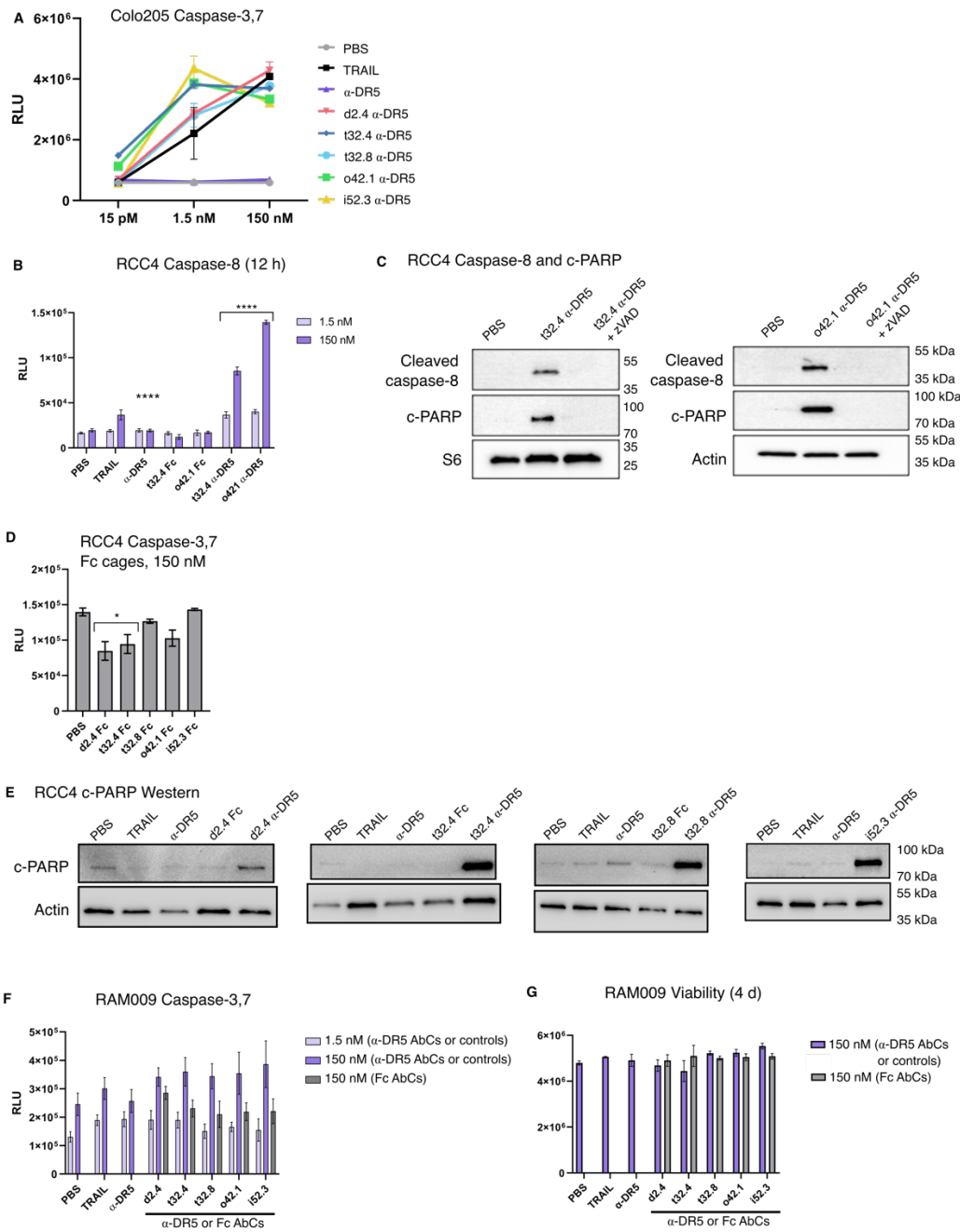


**Figure S8. Additional  $\alpha$ -DR5 AbC experiments.** **A**,  $\alpha$ -DR5 AbCs and TRAIL activate caspase-3,7 in Colo205 colorectal cancer cell lines. **B**,  $\alpha$ -DR5 o42.1 AbCs activate caspase-8 after 12 hour incubation in t32.4 and o42.1  $\alpha$ -DR5 AbCs **C**, Cleaved-caspase 8 and cleaved-PARP inhibition after 24 hour incubation with t32.4 and o42.1  $\alpha$ -DR5 AbCs, and 10  $\mu$ M zVAD, a caspase inhibitor (**C**). **D**, AbCs formed with Fc from hlgG1 do not activate caspase-3,7 at 150 nM in RCC4 cells. **E**, PARP is cleaved by  $\alpha$ -DR5 AbCs in RCC4 cells, but not by TRAIL,  $\alpha$ -DR5, or Fc AbCs. **F-G**,  $\alpha$ -DR5 AbCs do not greatly activate caspase-3,7 after 2 d (**F**) or reduce viability (**G**) in a primary tubular kidney cell line (RAM009). Statistical analyses are reported in Table S8.

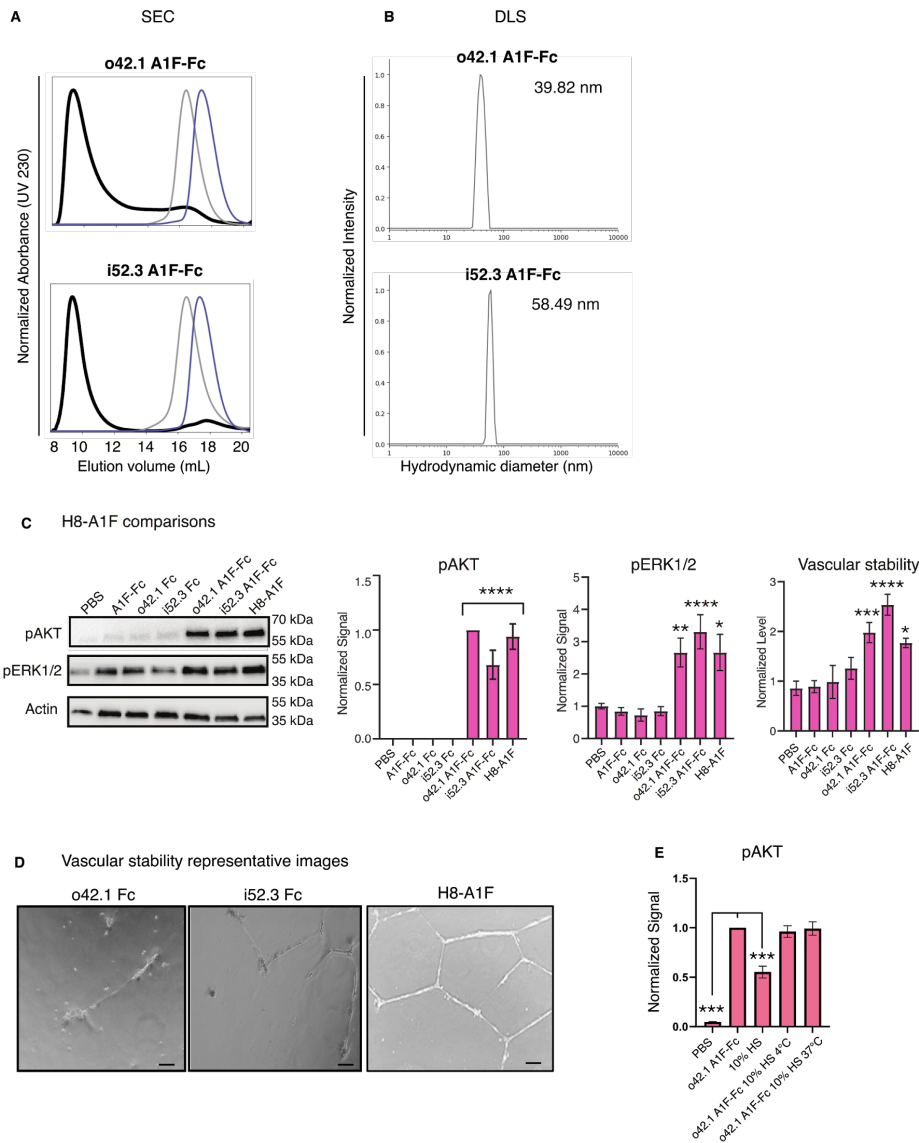


**Figure S9. Additional A1F-Fc AbC experiments.** **A-B**, o42.1 and i52.3 AbCs formed with A1F-Fc are monodisperse and of the expected size per SEC on a Superose 6 column (**A**) and DLS (**B**). SEC shows the assembly trace in black, the relevant AbC design component in grey, and the A1F-Fc in purple. **C**, A control assembly displaying 8 A1F ligands produced similar levels of pAKT and pERK1/2 activation along with a comparable increase in vascular stability. **D**, Representative images of o42.1 and i52.3 AbCs formed with Fc in the vascular stability assays. **E**, o42.1 A1F-Fc AbCs were incubated with 10% human serum (HS) for 24 hours at 4°C or 37°C and applied to HUVEC cells at 150 nM. pAKT signal showed no decrease from o42.1 A1F-Fc particles incubated with serum. Statistical analyses are reported in Table S9.

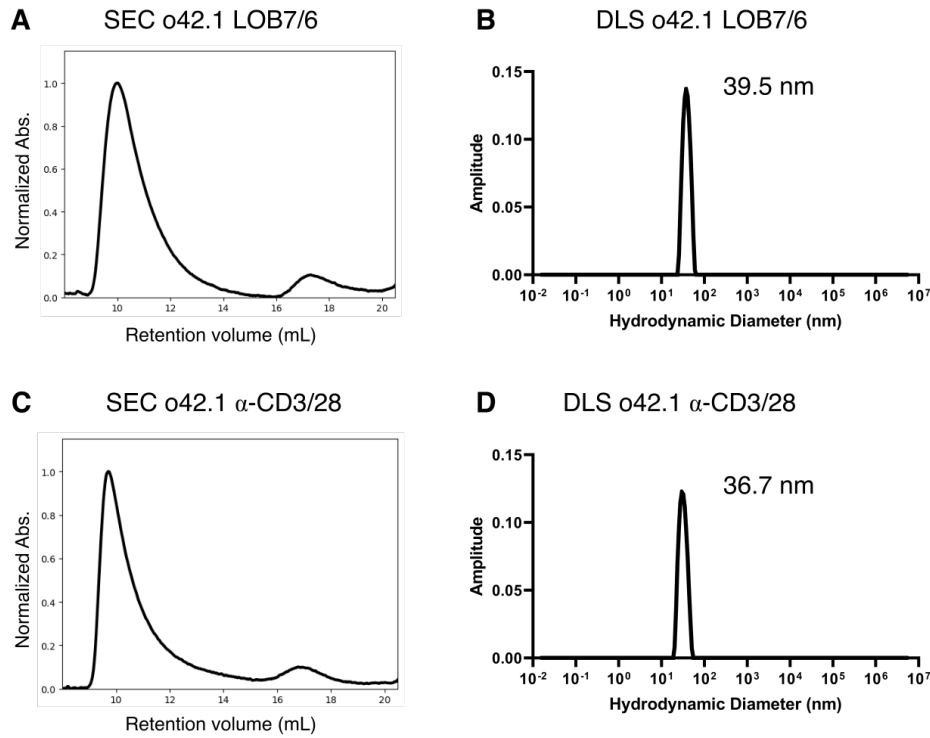


**Figure S10. Structural verification for immune stimulating AbCs (with  $\alpha$ -CD40 or  $\alpha$ -CD3/28).** **A-C**, Structural verification for  $\alpha$ -CD40 AbCs formed with o42.1 and LOB7/6, using SEC on a Superose 6 column (**A**), DLS (**B**), and NS-EM (**C**). **D-E**, Structural verification for  $\alpha$ -CD3/28 mosaic AbCs formed with o42.1, using SEC (**D**) and DLS (**E**). The excess peak corresponds on the right corresponds to unassembled component, likely o42.1 AbC-forming design (as excess was added).

5

10

15

20

25

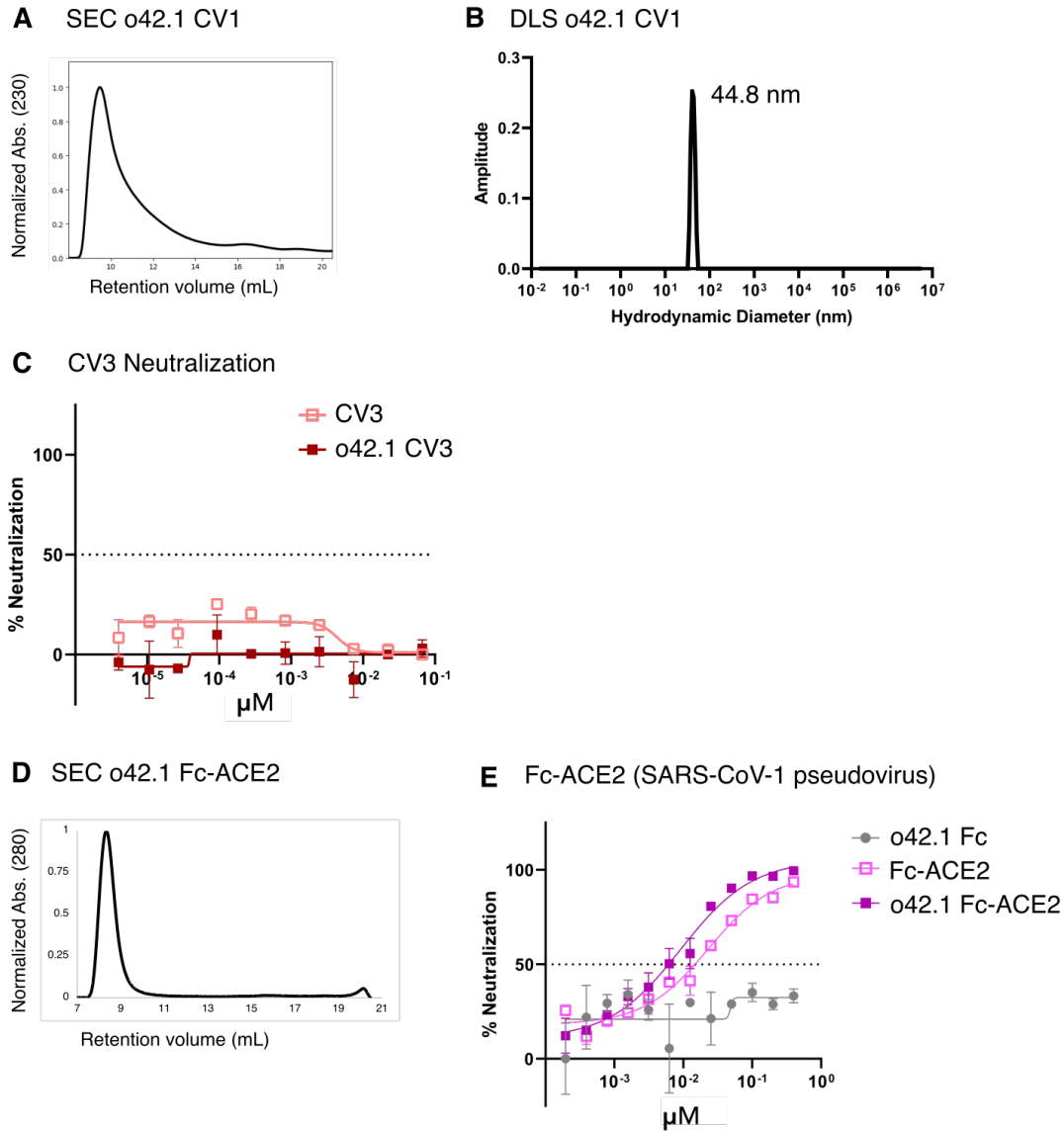


**Figure S11. Additional viral neutralization experiments.** **A-B**, Structural validation of o42.1 CV1 using SEC (**A**) and DLS (**B**). **C**, Neither o42.1 CV3 or free CV3 ( $\alpha$ -CoV-2 S IgG, 31) effectively neutralize SARS-CoV-2 pseudovirus. **D**, SEC characterization of o42.1 Fc-ACE2. **E**, o42.1 Fc-ACE2 is slightly more effective at neutralizing a SARS-CoV-1 pseudovirus compared to free Fc-ACE2.

5

10

## Supplemental Tables

**Table S1. Success rates of designed antibody-binding cage-forming oligomers.**

5 Solubility (column 2) refers to the presence of protein in the post-lysis, post-centrifugation, pre-IMAC soluble fraction as read out by SDS gel. Good SEC component (column 3) refers to SEC traces with some peak corresponding to the approximate predicted size of the nanocage-forming design model. Data for cage formation with Fc are shown in Fig. 2 and 3.

Geometry	# ordered	Soluble component	Good SEC component	Forms cage with Fc
D2 dihedron	6	5	4	3
T32 tetrahedron	11	8	7	2
O32 octahedron	4	3	3	0
O42 octahedron	2	1	1	1
I32 icosahedron	14	14	10	0
I52 icosahedron	11	11	10	2
Total	48	42	35	8

10

15

20

25

30

**Table S2. Structural properties of designed models from SAXS analyses.** AbC design model predicted data (model) is compared against experimentally-derived SAXS data (exp) for radius of gyration ( $R_g$ ) and  $d_{max}$ . The  $q_{max}$  used for analysis is reported. All data was analyzed using Scatter3.

5

Design	$R_g$ model (Å)	$R_g$ exp (Å)	$D_{max}$ model (Å)	$D_{max}$ exp (Å)	$q_{max}$ 1/nm
<b>d2.3</b>	60.69	71.8	210	217	0.21
<b>d2.4</b>	60.67	63.88	210	214	0.25
<b>d2.7</b>	58.95	59.2	197	199	0.25
<b>t32.4</b>	107.27	112.02	280	282	0.25
<b>t32.8</b>	94.39	108.22	263	278	0.17
<b>o42.1</b>	126.48	135.1	320	331	0.16
<b>i52.3</b>	167.73	175.76	427	409	0.15
<b>i52.6</b>	187.32	188.9	454	443	0.15
<b>d3.08</b>	56.34	55.16	164	159	0.20
<b>d3.36</b>	60.38	59.32	168	175	0.15

10

15

20

25



**Table S3.** Details on EM data acquisition of different AbC samples.

Sample name	Stain	Magnification	Pixel size (Å /pixel)	# Micrographs
d2.3 Fc	UF	67,000	1.6	300
d2.4 Fc	UF	67,000	1.6	234
d2.7 Fc	nano-W	67,000	1.6	251
t32.4 Fc	nano-W	67,000	1.6	359
t32.8 Fc	nano-W	67,000	1.6	739
o42.1 Fc	cryo	36,000	1.16	487
i52.3 Fc	cryo	36,000	1.16	460
i52.6 Fc	nano-W	52,000	2.07	342
d2.3 hlgG1	UF	67,000	1.6	331
d2.4 hlgG1	UF	67,000	1.6	160
d2.7 hlgG1	nano-W	67,000	1.6	206
t32.4 hlgG1	nano-W	67,000	1.6	346
t32.8 hlgG1	nano-W	67,000	1.6	193
o42.1 hlgG1	UF	67,000	1.6	525
i52.3 hlgG1	nano-W	52,000	2.07	391
i52.6 hlgG1	nano-W	52,000	2.07	282
D3-08 Fc	nano-W	57,000	2.52	88
D3-36 Fc	nano-W	57,000	2.52	93

**Table S4.** Details on EM data processing of different AbCs.

Sample name	Particle picking	CTF estimation	2D class averages	Ab initio reconstruction and symmetry applied	3D refinement and symmetry applied	# particle in final 3D map/total picked particles	Estimated resolution of 3D map (Å) (*)
d2.3 Fc	cisTEM	cisTEM	cisTEM	cisTEM, D2	cisTEM, D2	8295/11211	-
d2.4 Fc	DoG picker	GCTF	cryoSPARC	cryoSPARC, C1	cryoSPARC, C1	28562/46306	-
d2.7 Fc	cisTEM	cisTEM	cisTEM	cisTEM, D2	cisTEM, D2	17002/24441	-
t32.4 Fc	cisTEM	cisTEM	cisTEM	cisTEM, T2	cisTEM, T2	12416/16806	-
t32.8 Fc	cisTEM	cisTEM	cisTEM	cisTEM, T2	cisTEM, T2	7638/16147	-
o42.1 Fc (cryo-EM)	cryoSPARC Template picking	CTFFIND4 within cryoSPARC	cryoSPARC	cryoSPARC, C1	cryoSPARC, O	4032/16611	11.14
i52.3 Fc (cryo-EM)	cryoSPARC Template picking	CTFFIND4 within cryoSPARC	cryoSPARC	cryoSPARC, C1	cryoSPARC, I	3918/11076	12.18
i52.6 Fc	cisTEM	cisTEM	cisTEM	cisTEM, I2	cisTEM, I2	11801/26436	-
d2.3 hlgG1	cisTEM	cisTEM	cisTEM	-	-	-	-
d2.4 hlgG1	cisTEM	cisTEM	cisTEM	-	-	-	-
d2.7 hlgG1	cisTEM	cisTEM	cisTEM	-	-	-	-
t32.4 hlgG1	cisTEM	cisTEM	cisTEM	-	-	-	-
t32.8 hlgG1	cisTEM	cisTEM	cisTEM	-	-	-	-
o42.1 hlgG1	DoG picker	GCTF	cryoSPARC	-	-	-	-
i52.3 hlgG1	cisTEM	cisTEM	cisTEM	-	-	-	-

i52.6 hlgG1	cisTEM	cisTEM	Relion	-	-	-	-
D3-08 Fc	cisTEM	cisTEM	cisTEM	cisTEM, D3	cisTEM, D3	12322/80375	-
D3-36 Fc	cisTEM	cisTEM	cisTEM	cisTEM, D3	cisTEM, D3	16947/43301	-

(\*) Negative stain reconstructions obtained had resolution of  $\sim 20\text{\AA}$ .

5

10

15

20

25

30

35

**Table S5. Success rates of designed antibody-binding cage-forming oligomers using unvalidated building blocks** (see table S1 for descriptions of columns 3+4). Data for cage formation with Fc are shown in Fig. S5.

Geometry	# ordered	Soluble component	Good SEC component	Forms cage with Fc
D3 dihedron	14	9	3	2
T32 tetrahedron	11	10	2	0
O32 octahedron	15	12	3	0
I32 icosahedron	8	5	2	0
Total	48	36	10	2

5

10

15

20

25

30

35 **Table S6.** Details on dynamic light scattering data. Predicted diameters are estimated from computational models fit with appropriate ligands. Given the difficult-to-assess

flexibility associated with Fc-fusions to either functional ligands (A1F) or Fab domains, the estimates of these cages may not be accurate.

<b>AbC description</b>	<b>Figure</b>	<b>Predicted diameter from design (nm)</b>	<b>Hydrodynamic diameter (nm)</b>	<b>Standard deviation (nm)</b>
d2.3 Fc week 1	S5a	14.19	12.87	6.70
d2.3 Fc week 2	S5a	14.19	13.75	7.72
d2.3 Fc week 3	S5a	14.19	11.96	5.93
d2.4 Fc week 1	S5a	14.30	13.08	5.79
d2.4 Fc week 2	S5a	14.30	13.10	6.13
d2.4 Fc week 3	S5a	14.30	12.87	5.58
d2.7 Fc week 1	S5a	14.96	13.73	4.77
d2.7 Fc week 2	S5a	14.96	13.65	4.74
d2.7 Fc week 3	S5a	14.96	13.45	5.23
d2.7 Fc week 4	S5a	14.96	13.89	5.14
t32.4 Fc week 1	S5a	27.96	24.03	6.44
t32.4 Fc week 2	S5a	27.96	24.79	6.98
t32.4 Fc week 3	S5a	27.96	24.30	6.98
t32.4 Fc week 4	S5a	27.96	25.77	7.49
t32.8 Fc week 1	S5a	25.31	24.16	6.59
t32.8 Fc week 2	S5a	25.31	24.68	8.68
t32.8 Fc week 3	S5a	25.31	25.71	6.47
t32.8 Fc week 4	S5a	25.31	25.80	10.46
o42.1 Fc week 1	S5a	31.50	30.65	5.71
o42.1 Fc week 2	S5a	31.50	30.98	7.01
o42.1 Fc week 3	S5a	31.50	30.77	3.40

o42.1 Fc week 4	S5a	31.50	31.52	9.06
i52.3 Fc week 1	S5a	42.12	43.84	9.61
i52.3 Fc week 2	S5a	42.12	42.75	8.96
i52.3 Fc week 3	S5a	42.12	43.00	5.49
i52.3 Fc week 4	S5a	42.12	43.85	4.98
i52.6 Fc week 1	S5a	44.96	51.33	9.19
i52.6 Fc week 2	S5a	44.96	50.32	9.83
i52.6 Fc week 3	S5a	44.96	50.53	13.88
i52.6 Fc week 4	S5a	44.96	50.37	14.21
o42.1 A1F-Fc	S8b	38.25	39.82	25.24
i52.3 A1F-Fc	S8b	49.43	58.49	32.17
o42.1 LOB7/6 ( $\alpha$ -CD40)	S9b	40.40	79.52	20.21
o42.1 $\alpha$ -CD3/28	S9d	40.40	36.66	3.66
o42.1 CV1 ( $\alpha$ -CoV-2 S)	S10b	40.40	44.76	23.67

5

10

15

**Table S7. Statistical information for exchange experiments.**

Experiment (Fig.)	Condition	n	Test	Mean compared to	$\alpha$	Summary	Adjusted P value
Cage fraction 485 ex./ 510 em.	o42.1 GFP-Fc	3	1way ANOVA with post-hoc Dunnett	N/A	N/A	N/A	N/A
	RFP-Fc	3	1way ANOVA with post-hoc Dunnett	o42.1 GFP-Fc	0.05	****	<0.0001
	o42.1 pre- exchanged	3	1way ANOVA with post-hoc Dunnett	o42.1 GFP-Fc	0.05	****	<0.0001
	5 min o42.1 GFP-Fc + 25x RFP-Fc	3	1way ANOVA with post-hoc Dunnett	o42.1 GFP-Fc	0.05	****	<0.0001
	2 hr o42.1 GFP-Fc + 25x RFP-Fc	3	1way ANOVA with post-hoc Dunnett	o42.1 GFP-Fc	0.05	ns	0.9891
	4 hr o42.1 GFP-Fc + 25x RFP-Fc	3	1way ANOVA with post-hoc Dunnett	o42.1 GFP-Fc	0.05	ns	0.5186
	24 hr o42.1 GFP-Fc + 25x RFP-Fc	3	1way ANOVA with post-hoc Dunnett	o42.1 GFP-Fc	0.05	ns	0.0773
Cage fraction 558 ex./ 605 em.	o42.1 GFP-Fc	3	1way ANOVA with post-hoc Dunnett	N/A	N/A	N/A	N/A
	RFP-Fc	3	1way ANOVA with post-hoc Dunnett	o42.1 GFP-Fc	0.05	ns	0.7647
	o42.1 pre- exchanged	3	1way ANOVA with post-hoc Dunnett	o42.1 GFP-Fc	0.05	****	<0.0001
	5 min o42.1 GFP-Fc + 25x RFP-Fc	3	1way ANOVA with post-hoc Dunnett	o42.1 GFP-Fc	0.05	***	0.0004
	2 hr o42.1 GFP-Fc + 25x RFP-Fc	3	1way ANOVA with post-hoc Dunnett	o42.1 GFP-Fc	0.05	****	<0.0001

	4 hr o42.1 GFP-Fc + 25x RFP-Fc	3	1way ANOVA with post-hoc Dunnett	o42.1 GFP-Fc	0.05	****	<0.0001
	24 hr o42.1 GFP-Fc + 25x RFP-Fc	3	1way ANOVA with post-hoc Dunnett	o42.1 GFP-Fc	0.05	****	<0.0001

5

10

15

20

25

30

35



**Table S8. Statistical information for DR5 experiments.** All analyses were performed using Graphpad Prism Software.

Experiment (Fig.)	Condition	Concentration	n	Test	Mean compared to	$\alpha$	Summary	Adjusted P value
Caspase-3,7 RCC4 (4b)	PBS	15 pM	6	2way ANOVA with post-hoc Dunnett	N/A	N/A	N/A	N/A
		1.5 nM	6	2way ANOVA with post-hoc Dunnett	15 pM PBS	0.05	ns	0.9996
		150 nM	6	2way ANOVA with post-hoc Dunnett	15 pM PBS	0.05	ns	0.9994
	TRAIL	15 pM	6	2way ANOVA with post-hoc Dunnett	15 pM PBS	0.05	ns	0.9996
		1.5 nM	6	2way ANOVA with post-hoc Dunnett	15 pM PBS	0.05	ns	0.9996
		150 nM	6	2way ANOVA with post-hoc Dunnett	15 pM PBS	0.05	ns	0.9668
	$\alpha$ -DR5	15 pM	6	2way ANOVA with post-hoc Dunnett	15 pM PBS	0.05	ns	0.9997
		1.5 nM	6	2way ANOVA with post-hoc Dunnett	15 pM PBS	0.05	ns	>0.9999
		150 nM	6	2way ANOVA with post-hoc Dunnett	15 pM PBS	0.05	ns	0.2005
	d2.4 $\alpha$ -DR5	15 pM	6	2way ANOVA with post-hoc Dunnett	15 pM PBS	0.05	ns	0.9995

	1.5 nM	6	2way ANOVA with post-hoc Dunnett	15 pM PBS	0.05	ns	0.9988
	150 nM	6	2way ANOVA with post-hoc Dunnett	15 pM PBS	0.05	****	<0.0001
t32.4 $\alpha$ -DR5	15 pM	6	2way ANOVA with post-hoc Dunnett	15 pM PBS	0.05	ns	0.9998
	1.5 nM	6	2way ANOVA with post-hoc Dunnett	15 pM PBS	0.05	****	<0.0001
	150 nM	6	2way ANOVA with post-hoc Dunnett	15 pM PBS	0.05	****	<0.0001
t32.8 $\alpha$ -DR5	15 pM	3	2way ANOVA with post-hoc Dunnett	15 pM PBS	0.05	ns	0.984
	1.5 nM	3	2way ANOVA with post-hoc Dunnett	15 pM PBS	0.05	ns	0.6177
	150 nM	3	2way ANOVA with post-hoc Dunnett	15 pM PBS	0.05	****	<0.0001
o42.1 $\alpha$ -DR5	15 pM	6	2way ANOVA with post-hoc Dunnett	15 pM PBS	0.05	ns	0.9991
	1.5 nM	6	2way ANOVA with post-hoc Dunnett	15 pM PBS	0.05	****	<0.0001
	150 nM	6	2way ANOVA with post-hoc Dunnett	15 pM PBS	0.05	****	<0.0001

		15 pM	3	2way ANOVA with post-hoc Dunnett	15 pM PBS	0.05	ns	0.9442
	i52.3 $\alpha$ -DR5	1.5 nM	3	2way ANOVA with post-hoc Dunnett	15 pM PBS	0.05	ns	0.8227
		150 nM	3	2way ANOVA with post-hoc Dunnett	15 pM PBS	0.05	****	<0.0001
Viability 4d RCC4 (4c)	PBS	150 nM	3	1way ANOVA with post-hoc Dunnett	N/A	N/A	N/A	N/A
	TRAIL	150 nM	3	1way ANOVA with post-hoc Dunnett	PBS	0.05	ns	0.5207
	$\alpha$ -DR5	150 nM	3	1way ANOVA with post-hoc Dunnett	PBS	0.05	ns	0.9996
	d2.4 $\alpha$ -DR5	150 nM	3	1way ANOVA with post-hoc Dunnett	PBS	0.05	*	0.0238
	t32.4 $\alpha$ -DR5	150 nM	3	1way ANOVA with post-hoc Dunnett	PBS	0.05	****	<0.0001
	t32.8 $\alpha$ -DR5	150 nM	3	1way ANOVA with post-hoc Dunnett	PBS	0.05	****	<0.0001
	o42.1 $\alpha$ -DR5	150 nM	3	1way ANOVA with post-hoc Dunnett	PBS	0.05	****	<0.0001
	i52.3 $\alpha$ -DR5	150 nM	3	1way ANOVA with post-hoc Dunnett	PBS	0.05	**	0.0079

Viability 4d RCC4 Fc cages (4d)	PBS	150 nM	3	1way ANOVA with post-hoc Dunnett	N/A	N/A	N/A	N/A
	d2.4 Fc	150 nM	3	1way ANOVA with post-hoc Dunnett	PBS	0.05	ns	0.7157
	t32.4 Fc	150 nM	3	1way ANOVA with post-hoc Dunnett	PBS	0.05	ns	0.9976
	t32.8 Fc	150 nM	3	1way ANOVA with post-hoc Dunnett	PBS	0.05	ns	0.8556
	o42.1 Fc	150 nM	3	1way ANOVA with post-hoc Dunnett	PBS	0.05	ns	0.2309
	i52.3 Fc	150 nM	3	1way ANOVA with post-hoc Dunnett	PBS	0.05	ns	0.9302
Viability 6d RCC4 (4e)	PBS	150 nM	6	1way ANOVA with post-hoc Dunnett	N/A	N/A	N/A	N/A
	TRAIL	150 nM	6	1way ANOVA with post-hoc Dunnett	PBS	0.05	ns	0.9996
	$\alpha$ -DR5	150 nM	6	1way ANOVA with post-hoc Dunnett	PBS	0.05	ns	>0.9999
	t32.4 Fc	150 nM	3	1way ANOVA with post-hoc Dunnett	PBS	0.05	ns	0.9591
	o42.1 Fc	150 nM	3	1way ANOVA with post-hoc Dunnett	PBS	0.05	ns	0.9593

	t32.4 $\alpha$ -DR5	150 nM	6	1way ANOVA with post-hoc Dunnett	PBS	0.05	****	<0.0001
	o42.1 $\alpha$ -DR5	150 nM	6	1way ANOVA with post-hoc Dunnett	PBS	0.05	***	0.0001
c-PARP quant. (4g)	PBS	150 nM	4	1way ANOVA with post-hoc Dunnett	N/A	N/A	N/A	N/A
	TRAIL	150 nM	4	1way ANOVA with post-hoc Dunnett	PBS	0.05	ns	0.0845
	$\alpha$ -DR5	150 nM	3	1way ANOVA with post-hoc Dunnett	PBS	0.05	ns	0.4746
	o42.1 Fc	150 nM	3	1way ANOVA with post-hoc Dunnett	PBS	0.05	ns	0.9979
	o42.1 $\alpha$ -DR5	150 nM	3	1way ANOVA with post-hoc Dunnett	PBS	0.05	****	<0.0001
Caspase-3,7 Colo205 (S7a)		15 pM	2	2way ANOVA with post-hoc Dunnett	N/A	N/A	N/A	N/A
	PBS	1.5 nM	2	2way ANOVA with post-hoc Dunnett	15 pM PBS	0.05	ns	>0.9999
		150 nM	2	2way ANOVA with post-hoc Dunnett	15 pM PBS	0.05	ns	>0.9999
	TRAIL	15 pM	2	2way ANOVA with post-hoc Dunnett	15 pM PBS	0.05	ns	>0.9999

	1.5 nM	2	2way ANOVA with post-hoc Dunnett	15 pM PBS	0.05	***	0.0006
	150 nM	2	2way ANOVA with post-hoc Dunnett	15 pM PBS	0.05	****	<0.0001
α-DR5	15 pM	2	2way ANOVA with post-hoc Dunnett	15 pM PBS	0.05	ns	0.9997
	1.5 nM	2	2way ANOVA with post-hoc Dunnett	15 pM PBS	0.05	ns	>0.9999
	150 nM	2	2way ANOVA with post-hoc Dunnett	15 pM PBS	0.05	ns	0.9996
d2.4 α-DR5	15 pM	2	2way ANOVA with post-hoc Dunnett	15 pM PBS	0.05	ns	0.9996
	1.5 nM	2	2way ANOVA with post-hoc Dunnett	15 pM PBS	0.05	****	<0.0001
	150 nM	2	2way ANOVA with post-hoc Dunnett	15 pM PBS	0.05	****	<0.0001
t32.4 α-DR5	15 pM	2	2way ANOVA with post-hoc Dunnett	15 pM PBS	0.05	ns	0.1074
	1.5 nM	2	2way ANOVA with post-hoc Dunnett	15 pM PBS	0.05	****	<0.0001
	150 nM	2	2way ANOVA with post-hoc Dunnett	15 pM PBS	0.05	****	<0.0001

		15 pM	2	2way ANOVA with post-hoc Dunnett	15 pM PBS	0.05	ns	>0.9999
	t32.8 $\alpha$ -DR5	1.5 nM	2	2way ANOVA with post-hoc Dunnett	15 pM PBS	0.05	****	<0.0001
		150 nM	2	2way ANOVA with post-hoc Dunnett	15 pM PBS	0.05	****	<0.0001
		15 pM	2	2way ANOVA with post-hoc Dunnett	15 pM PBS	0.05	ns	0.6538
	o42.1 $\alpha$ -DR5	1.5 nM	2	2way ANOVA with post-hoc Dunnett	15 pM PBS	0.05	****	<0.0001
		150 nM	2	2way ANOVA with post-hoc Dunnett	15 pM PBS	0.05	****	<0.0001
		15 pM	2	2way ANOVA with post-hoc Dunnett	15 pM PBS	0.05	ns	>0.9999
	i52.3 $\alpha$ -DR5	1.5 nM	2	2way ANOVA with post-hoc Dunnett	15 pM PBS	0.05	****	<0.0001
		150 nM	2	2way ANOVA with post-hoc Dunnett	15 pM PBS	0.05	****	<0.0001
Caspase-8 RCC4 12 h (S7b)	PBS	1.5 nM	6	2way ANOVA with post-hoc Dunnett	1.5 nM PBS	0.05	N/A	N/A
		150 nM	6	2way ANOVA with post-hoc Dunnett	1.5 nM PBS	0.05	ns	0.9909

TRAIL	1.5 nM	6	2way ANOVA with post-hoc Dunnett	1.5 nM PBS	0.05	ns	0.999
	150 nM	6	2way ANOVA with post-hoc Dunnett	1.5 nM PBS	0.05	****	<0.0001
$\alpha$ -DR5	1.5 nM	6	2way ANOVA with post-hoc Dunnett	1.5 nM PBS	0.05	ns	0.9918
	150 nM	6	2way ANOVA with post-hoc Dunnett	1.5 nM PBS	0.05	ns	0.9955
t32.4 Fc	1.5 nM	6	2way ANOVA with post-hoc Dunnett	1.5 nM PBS	0.05	ns	>0.9999
	150 nM	6	2way ANOVA with post-hoc Dunnett	1.5 nM PBS	0.05	ns	0.9048
o42.1 Fc	1.5 nM	6	2way ANOVA with post-hoc Dunnett	1.5 nM PBS	0.05	ns	>0.9999
	150 nM	6	2way ANOVA with post-hoc Dunnett	1.5 nM PBS	0.05	ns	0.9997
t32.4 $\alpha$ -DR5	1.5 nM	6	2way ANOVA with post-hoc Dunnett	1.5 nM PBS	0.05	****	<0.0001
	150 nM	6	2way ANOVA with post-hoc Dunnett	1.5 nM PBS	0.05	****	<0.0001
o42.1 $\alpha$ -DR5	1.5 nM	6	2way ANOVA with post-hoc Dunnett	1.5 nM PBS	0.05	****	<0.0001



		150 nM	6	2way ANOVA with post-hoc Dunnett	1.5 nM PBS	0.05	****	<0.0001
Caspase- 3,7 RCC4 Fc cages (S7d)	PBS	150 nM	3	1way ANOVA with post-hoc Dunnett	N/A	N/A	N/A	N/A
	d2.4 Fc	150 nM	6	1way ANOVA with post-hoc Dunnett	PBS	0.05	*	0.0129
	t32.4 Fc	150 nM	6	1way ANOVA with post-hoc Dunnett	PBS	0.05	*	0.046
	t32.8 Fc	150 nM	3	1way ANOVA with post-hoc Dunnett	PBS	0.05	ns	0.9198
	o42.1 Fc	150 nM	6	1way ANOVA with post-hoc Dunnett	PBS	0.05	ns	0.2112
	i52.3 Fc	150 nM	3	1way ANOVA with post-hoc Dunnett	PBS	0.05	ns	0.9996
RAM009 Caspase- 3,7 (S7f)	PBS	1.5 nM	6	2way ANOVA with post-hoc Dunnett	PBS	0.05	N/A	N/A
		150 nM	6	2way ANOVA with post-hoc Dunnett	PBS	0.05	ns	0.3848
	TRAIL	1.5 nM	6	2way ANOVA with post-hoc Dunnett	PBS	0.05	ns	0.9726
		150 nM	6	2way ANOVA with post-hoc Dunnett	PBS	0.05	ns	0.0525

α-DR5	1.5 nM	6	2way ANOVA with post-hoc Dunnett	PBS	0.05	ns	0.9566
	150 nM	6	2way ANOVA with post-hoc Dunnett	PBS	0.05	ns	0.2752
d2.4 α-DR5	1.5 nM	6	2way ANOVA with post-hoc Dunnett	PBS	0.05	ns	0.9677
	150 nM	6	2way ANOVA with post-hoc Dunnett	PBS	0.05	**	0.0076
t32.4 α-DR5	1.5 nM	6	2way ANOVA with post-hoc Dunnett	PBS	0.05	ns	0.9703
	150 nM	6	2way ANOVA with post-hoc Dunnett	PBS	0.05	**	0.0028
t32.8 α-DR5	1.5 nM	6	2way ANOVA with post-hoc Dunnett	PBS	0.05	ns	0.9996
	150 nM	6	2way ANOVA with post-hoc Dunnett	PBS	0.05	**	0.0067
o42.1 α-DR5	1.5 nM	6	2way ANOVA with post-hoc Dunnett	PBS	0.05	ns	0.9991
	150 nM	6	2way ANOVA with post-hoc Dunnett	PBS	0.05	**	0.0038
i52.3 α-DR5	1.5 nM	6	2way ANOVA with post-hoc Dunnett	PBS	0.05	ns	0.9994

		150 nM	6	2way ANOVA with post-hoc Dunnett	PBS	0.05	***	0.0006
	d2.4 Fc	150 nM	6	2way ANOVA with post-hoc Dunnett	PBS	0.05	ns	0.9966
	t32.4 Fc	150 nM	6	2way ANOVA with post-hoc Dunnett	PBS	0.05	ns	0.9997
	t32.8 Fc	150 nM	6	2way ANOVA with post-hoc Dunnett	PBS	0.05	ns	0.9992
	o42.1 Fc	150 nM	6	2way ANOVA with post-hoc Dunnett	PBS	0.05	ns	0.9994
	i52.3 Fc	150 nM	6	2way ANOVA with post-hoc Dunnett	PBS	0.05	ns	0.9995
RAM009 Viability (S7g)	PBS	150 nM	6	2way ANOVA with post-hoc Dunnett	PBS	0.05		
	TRAIL	150 nM	3	2way ANOVA with post-hoc Dunnett	PBS	0.05	ns	0.9901
	$\alpha$ -DR5	150 nM	3	2way ANOVA with post-hoc Dunnett	PBS	0.05	ns	0.9995
	d2.4 $\alpha$ -DR5	150 nM	3	2way ANOVA with post-hoc Dunnett	PBS	0.05	ns	0.9996
	t32.4 $\alpha$ -DR5	150 nM	3	2way ANOVA with post-hoc Dunnett	PBS	0.05	ns	0.9212

t32.8 $\alpha$ -DR5	150 nM	3	2way ANOVA with post-hoc Dunnett	PBS	0.05	ns	0.7875
o42.1 $\alpha$ - DR5	150 nM	3	2way ANOVA with post-hoc Dunnett	PBS	0.05	ns	0.7485
i52.3 $\alpha$ -DR5	150 nM	3	2way ANOVA with post-hoc Dunnett	PBS	0.05	ns	0.1419
d2.4 Fc	150 nM	3	2way ANOVA with post-hoc Dunnett	PBS	0.05	ns	0.9996
t32.4 Fc	150 nM	3	2way ANOVA with post-hoc Dunnett	PBS	0.05	ns	0.9718
t32.8 Fc	150 nM	3	2way ANOVA with post-hoc Dunnett	PBS	0.05	ns	0.999
o42.1 Fc	150 nM	3	2way ANOVA with post-hoc Dunnett	PBS	0.05	ns	0.9913
i52.3 Fc	150 nM	3	2way ANOVA with post-hoc Dunnett	PBS	0.05	ns	0.9837

5

10

**Table S9. Statistical information for A1F-Fc experiments.** All analyses were performed using Graphpad Prism Software.

Experiment (Fig.)	Condition	n	Test	Mean compared to	$\alpha$	Summary	Adjusted P value
pAKT (4j, S8c (H8))	PBS	13	1way ANOVA with post-hoc Dunnett	N/A	N/A	N/A	N/A
	A1F-Fc	3	1way ANOVA with post-hoc Dunnett	PBS	0.05	ns	>0.9999
	o42.1 Fc	4	1way ANOVA with post-hoc Dunnett	PBS	0.05	ns	>0.9999
	i52.3 Fc	3	1way ANOVA with post-hoc Dunnett	PBS	0.05	ns	>0.9999
	o42.1 A1F-Fc	9	1way ANOVA with post-hoc Dunnett	PBS	0.05	****	<0.0001
	i52.3 A1F-Fc	8	1way ANOVA with post-hoc Dunnett	PBS	0.05	****	<0.0001
	H8-A1F	4	1way ANOVA with post-hoc Dunnett	PBS	0.05	****	<0.0001
pERK1-2 (4j; S8c (H8))	PBS	13	1way ANOVA with post-hoc Dunnett	N/A	N/A	N/A	N/A
	A1F-Fc	3	1way ANOVA with post-hoc Dunnett	PBS	0.05	ns	0.9997
	o42.1 Fc	4	1way ANOVA with post-hoc Dunnett	PBS	0.05	ns	0.9955
	i52.3 Fc	3	1way ANOVA with post-hoc Dunnett	PBS	0.05	ns	0.9997
	o42.1 A1F-Fc	9	1way ANOVA with post-hoc Dunnett	PBS	0.05	**	0.0015
	i52.3 A1F-Fc	8	1way ANOVA with post-hoc Dunnett	PBS	0.05	***	0.0004
	H8-A1F	6	1way ANOVA with post-hoc Dunnett	PBS	0.05	ns	0.4766
Vascular stability (4k; S8c (H8))	PBS	7	1way ANOVA with post-hoc Dunnett	N/A	N/A	N/A	N/A
	A1F-Fc	6	1way ANOVA with post-hoc Dunnett	PBS	0.05	ns	0.9998
	o42.1 Fc	4	1way ANOVA with post-hoc Dunnett	PBS	0.05	ns	0.9946

	i52.3 Fc	3	1way ANOVA with post-hoc Dunnett	PBS	0.05	ns	0.6157
	o42.1 A1F-Fc	6	1way ANOVA with post-hoc Dunnett	PBS	0.05	***	0.0004
	i52.3 A1F-Fc	5	1way ANOVA with post-hoc Dunnett	PBS	0.05	****	<0.0001
	H8-A1F	4	1way ANOVA with post-hoc Dunnett	PBS	0.05	*	0.011
pAKT (10% HS exp.; S8e)	PBS	3	1way ANOVA with post-hoc Dunnett	o42.1 A1F-Fc	0.05	***	<0.0001
	o42.1 A1F-Fc	3	1way ANOVA with post-hoc Dunnett	o42.1 A1F-Fc	0.05	N/A	N/A
	10% HS	3	1way ANOVA with post-hoc Dunnett	o42.1 A1F-Fc	0.05	***	0.0002
	o42.1 A1F-Fc 10% HS 4°C	3	1way ANOVA with post-hoc Dunnett	o42.1 A1F-Fc	0.05	ns	0.9431
	o42.1 A1F-Fc 10% HS 37°C	3	1way ANOVA with post-hoc Dunnett	o42.1 A1F-Fc	0.05	ns	0.9998

5

10

15

20

**Table S10. EC50s from CD40 activation experiments.** EC50 values were interpolated from the response curves determined using the log(agonist) vs. response -- Variable slope (four parameters) fit using Graphpad Prism Software

	<b>IC50 log(uM)</b>	<b>95% CI log(uM)</b>
o42.1 IgG control	~ -1.455	(Very wide)
α-CD40	1.466	1.247 to 1.833
LOB7/6	~ -1.650	(Very wide)
o42.1 LOB7/6	0.1134	-0.001058 to ???

5

10

15

20

25

30

35

**Table S11. IC50s from SARS-CoV neutralization experiments.** IC50 values were interpolated from the neutralization curves determined using the log(inhibitor) vs. response -- Variable slope (four parameters) fit using Graphpad Prism Software

5

<b>SARS-CoV-2 pseudovirus neutralization</b>		
	<b>IC50 log(uM)</b>	<b>95% CI log(uM)</b>
CV1	-1.201	-1.935 to ???
o42.1 CV1	-3.566	??? to -3.044
CV30	-3.301	-3.464 to -3.141
o42.1 CV30	-3.716	-3.914 to -3.556
CV3	~ -2.591	(Very wide)
o42.1 CV3	-4.449	???
o42.1 Fc	-2.068	???
Fc-ACE2	-1.768	-2.016 to -1.483
o42.1 Fc-ACE2	-2.655	-2.740 to -2.589
<b>SARS-CoV-1 pseudovirus neutralization</b>		
	<b>IC50 log(uM)</b>	<b>95% CI log(uM)</b>
o42.1 Fc	~ 1.631e+015	~ 1.631e+015
Fc-ACE2	-1.642	-1.642
o42.1 Fc-ACE2	-2.039	-2.039

10

15



**Table S12. List of antibodies formed into cages as verified by at minimum size exclusion chromatography.** Successfully formed cages (by SEC) listed by the antibody target reactivity, antibody species and isotype, and designs used

<b>Ab reactivity</b>	<b>Ab subclass</b>	<b>Designs (validated by SEC at minimum)</b>	<b>Comments</b>
$\alpha$ -CD3	mIgG2a	t32.4, o42.1	OKT3
$\alpha$ -CD4	mIgG2b	o42.1	OKT4
$\alpha$ -CD28	hIgG1	t32.4, o42.1	CD28.6
$\alpha$ -CD40	mIgG2a or mIgG2b	o42.1	LOB7/6 or 82111 (respectively)
$\alpha$ -CoV2 S	hIgG1	o42.1	CV1, CV3, CV30
$\alpha$ -DR5 (human)	hIgG1	d2.3, d2.4, d2.7, t32.4, t32.8, o42.1, i52.3, i52.6	conatumumab
$\alpha$ -DR5 (mouse)	Armenian hamster IgG	t32.4, o42.1	MD5-1
$\alpha$ -EGFR	hIgG1	mIgG2b	cetuximab
$\alpha$ -LRP6	hIgG1	t32.4, o42.1	YW210.09
$\alpha$ -RSV F	hIgG1	d2.3, d2.4, d2.7, t32.4, t32.8, o42.1, i52.3, i52.6	mpe8
Non-specific	Rabbit IgG	d2.4, o42.1	Rabbit serum IgG

5

10

15

20

**Table S13. List of Fc-fusions formed into cages as verified by at minimum size exclusion chromatography.** Successfully formed cages (by SEC) listed by the ligand that was fused to Fc, the Fc sequence species and isotype, and designs used

5

<b>Fc-fusion ligand</b>	<b>Fc subclass</b>	<b>Designs (validated by SEC at minimum)</b>	<b>Comments</b>
Angiopoietin-1 F-domain	hIgG1	d2.4, t32.4, t32.8, o42.1, i52.3	
Angiotensin-converting enzyme 2 (ACE2)	hIgG1	o42.1	
CD80	hIgG1	o42.1	
mRuby2	hIgG1	d2.4, t32.4, t32.8, o42.1, i52.3	
sfGFP	hIgG1	d2.4, t32.4, t32.8, o42.1, i52.3	
VEGF-a	hIgG1	t32.4, o42.1	
VEGF-c	hIgG1	t32.4, o42.1	

10

15

20

25

**Table S14.** Amino acid sequences of all successful AbC-forming designs.

Name	Sequence
d2.3	MSDEEERNELIKRIREAAQRAREAAERTGDPRVRELARELARIAQIAFYLVLHDPSSSEVNEALKAVVKAIELAVRALEEAEK TGDPEVRELAREVVRLAVEVATATAAGENDTLRKAERALRLAKEAAKRGDAKAAKQAAKIAKLAANAGDEDVLKVKVELV RLAIELVEIVVENAKRKGDDDDKEAAEAALAAFRIVLAAAQLAGIASLEVLELALRLIKEVVENAQREGYDIAVAAAIAAVAFVAV AVAAAAADITSSEVLELAIRLIKEVVENAQREGYVILLAAALAAAAAFVVVAAAAKRAGITSSETLKRAIEEIRKRVVEEAQREGND ISEAARQAAEEFRKKAEEELKGSLEHHHHHH
d2.4	MSDEEERNELIKRIREAAQRAREAAERTGDPRVRELARELARIAQIAFYLVLHDPSSSEVNEALKAVVKAIELAVRALEAAEK TGDPRVRELAREVVKAADVAAEAQAGLNDKLREVAEKALRLAKEALKEGDSTAELAAEIARLAAKLAGDEDVLKVKVLLV EAIKLVKIVVENAKRKGDDSKAAEAFAAFVLAALAGIASEEVLELAARLIKEVVENAQREGYDIAVAAAIAAVAFVAVV VAAAAADITSSEVLELAIRLIKEVVENAQREGYVILLAAALAAAAAFVVVAAAAKRAGITSSETLKRAIEEIRKRVVEEAQREGNDI SEAARQAAEEFRKKAEEELKGSLEHHHHHH
d2.7	MSDEEERNELIKRIREAAQRAREAAERTGDPRVRELARELAKLAQIAFYLVLHDPSSAKEVNLALIVKAIELAVRALEEAEKT GDPHARELAREIVRLAVELARAVAAEAEEAKKQGNSELAEQVARAAQVALEVIKAAITAAKQGDRKAFRAALELVLEVIKAI EAVKQGNPKKVAEVALKAEIIRIVVQNAANKGDDADEAVEAARAFAEIVLAAAQLAGIDSEEVLELAARLIKEVVENAQREGY DIAVAAAIAAVAFVAVVAAAAADITSSEVLELAIRLIKEVVENAVREGYVILLAAALAAAAAFVVVAAAAKRAGITSSETLKRAIE EIRKRVVEEAQREGNDISEAARQAAEEFRKKAEEELKGSLEHHHHHH
t32.4	MFNKSQQSAFYLLNMPNLNEAQRNGFIQSLKDDPSKSEVVAGEAAIEAARNALKKGSPETAREAVRLALELVQEAEERQAR KTGSTERLIAAKLAIEVARVALKVGSPETAREAVRTALELVQELIRQARKTGSKEVLEEAALALEVAKVAEAVGSPETAAR AVATAVEALKEAGASEDEIAEIVARVISEVIRILKESGSEYKVICRAVARIVAEIVEALKRSGTSEDEIAEIVARVISEVIRTLKES GSDYLIICVCVAIIVAEIVEALKRSGTSEDEIAEIVARVISEVIRTLKESGSSYEVIKECVQIIVLAILALMKSGTEVEEILLILLRVK TEVRRTLKESGSLEHHHHHH
t32.8	MFNKDQQSAFYELNMPNLNEAQRNGFIQSLKDDPSQSLKILIKAAAGGDSELEEVAKRIVKELAEQGRSEKEAAKEAAELI ERITRAAGGNSDLIELAVRIVKILEEQGRSPSEAAKEAVEAIEAIVRAAGGDSEAIKVAEEIAKTIITQKESGSEYKEICRTVARI VAEIVEKLRNGASEDEIAEIVAAIIAAVILTLKLSGSDYLIICVCVAIIVAEIVEALKRSGTSEDEIAEIVARVISAVIRVLKESGSS YEVIKECVQIIVLAILALMKSGTEVEEILLILLRVKTEVRRTLKESGSLEHHHHHH
o42.1	MFNKDQQSAFYELNMPNLNEALRNGFIQLLKDDPSKSTVILTAAKVAAELSEKIRTLKESGSSYEQIAETVAKAVAKLVEKLLK RNGVSEDEIALAVALIISAVIQTLEKSGSSYEIVAEIVARIVAEIVEALKRSGTSEDEIAEIVARVISEVIRTLKESGSSYEIVAEIV ARIVAEIVEALKRSGTSEDEIAKIVARVIAEVLRTLKESGSSSEVIKEIVARIITEIKEALKRSGTSEDEIELITLMIEAALEIAKLS SGSEYEEICEDVARRIAELVEKLRDGTSAVEIAKIVAAIISAVIAMLKASGSSYEVICECVARIVAEIVEALKRSGTSAIIIALIVA LVISEVIRTLKESGSSFEVILECVIRIVLEIIEALKRSGTSEQDVMLIVMAVLLVVLATLQLSGSLEHHHHHH
i52.3	MSDEEERNELIKRIREAAQRAREAAERTGDPRVRELARELARLAQRAFYLVLHDPSSSDVNEALKLIVEAIEAAVRALEAAE RAGDPELREDAREAVRLAVEAAEEVQRNPSSSTANLLLKAIVALAEALAAAANGDKEKFKKAAESALEIAKRVEVASKEGD PEAVLEAAKVALRVAELAANKGDKEVFKKAAESALEVAKRLVEVASKEGDPELVLEAAKVALRVAELAANKGDKEVFKKAA ASAVEVALRLTEVASKEGDSELETEAAKVITRVRELASKQGDAAVAILAETAEVKLEIEESKRPQSESAKNLILIMQLLINQIR LLVLQIRMLDEQRQEGSLEHHHHHH
i52.6	MSDEEERNELIKRIREAAQRAREAAERTGDPRVRELARELARLAQRAFYLVLHDPSSSDVNEALKLIVEAIEAAVRALEAAE RTGDPKVREEARELVRRAVEAAEEVQRNPSSSEVNEKLKAIIVEIEVKVASLEAKEVTDPAKALKIAKKVIELALEAVKENPS TEALRAVLEAVRLASEVAKRVTPDKALKIAKLVIELALEAVKEDPSTDALRAVLEAVRLASEVAKRVTPDKALKIAKLVLEL AAEAVKEDPSTDALRAAKEAERLATEVAKRVTPDKKAREIEMLVLKLQMEAILAETEEVKKEIEESKRPQSESAKNLILIMQ LLINQIRLLALQIRMLALQLQEGSLEHHHHHH
D3-08	MSDEEERNELIKRIREAAQRAREAAERTGDPRVRELARELARLAQIMFYLVLHDPSSAKFVNEALKVVMEMIAVRALEKAE RIGDPEMREMARELVRAAVEMADLMTRAEEARRDPDSSDVNEALKLIREAIEAAKRALEAAERTGDPEVLRLLAILMELAV LAARLVQLDPSASDANEALKKIVEAIERAVRALEKAERTGDPEEREKARQKVAEAVVEAALILAEALRVAEKAAKNGDKEL FKKAAELALKVARLLVEVASKAGAPEFVLAEEIAIAVLELAVKQGDVDRVALLAAATALFVLMMAARVLFVFEAGGWLEHHHHHH H
D3-36	MFNKDQQSAFYELNLPKLEEFNRNGFIQALKTAPLASEAILGAAKMAAKATDEEVRVRLLEVRELARLFTEAERSNDDEC RRLAELAIKAVSLLMKAIEIATDEEEIRRLAEEARELIRLAQEAACRSNDDDELTKAAMFVAEMIAKAARETGDDKVLAEALRL EARLIVELAELKACKRGNSEAAERASELAQRVLEKARKVSEEAAREQGDDEVLLALALIALAVLALAEVACCRGNKEEAERAY KDAQRVLLLEAILVALKALLQGDEEVARLAQEAALAEALDHVQECRGGWLSVLEHHHHHH

**Table S15.** Amino acid sequences of Fc and Fc-fusions.

Name	Sequence
Fc	METDTLLLWVLLLWVPGSTGHHHHHHGGSENLYFQGGSEPKSSDKTHTCPPCPAPELLGGPSVFLFPPKPKDTLMISRTPEVTCVVDVSHEDPEVKFNWYVDGVEVHNAKTKPREEQYNSTYRVVSVLTVLHQDWLNGKEYKCKVSNKALPAPIEKTISKAKGQPREPQVYTLPPSRDELTKNQVSLTCLVKGFYPSDIAVEWESNGQPENNYKTPPVLDSDGSFFLYSKLTVDKSRWQQGNVFSCSVMHEALHNHYTQKSLSLSPGK
GFP-Fc (sfGFP)	SRATMETDTLLLWVLLLWVPGSTGHHHHHHGGSENLYFQGGSSKGEELFTGVVPIVELDGDVNGHKFSVRGEGEGDATNGKLTCLKFICTTGKLPVWPVTLVTTLYGVQCFSRYPDHMKRHDFFKSAMPEGYVQERTISFKDDGYKTRAEVKFEGD TLVNRIELKGIDFKEDGNILGHKLEYNFSHNVIYITADKQKNGIKANFKIRHNVEDGSVQLADHYQQNTPIGDGPVLLPDNHYLSTQSVLSKDPNEKRDHMLLEFVTAAGITHGMDELYKGGSGSEPKSSDKTHTCPPCPAPELLGGPSVFLFPPKPKDTLMISRTPEVTCVVDVSHEDPEVKFNWYVDGVEVHNAKTKPREEQYNSTYRVVSVLTVLHQDWLNGKEYKCKVSNKALPAPIEKTISKAKGQPREPQVYTLPPSRDELTKNQVSLTCLVKGFYPSDIAVEWESNGQPENNYKTPPVLDSDGSFFLYSKLTVDKSRWQQGNVFSCSVMHEALHNHYTQKSLSLSPGK
RFP-Fc (mRuby 2)	SRATMETDTLLLWVLLLWVPGSTGHHHHHHGGSENLYFQGGSVKGEELIKENMRMKVVMESVNGHQFKCTGEGEGENPYMGTQTMRIKVIEGGPLPFAFDILATSFMYGSRTFIKYPKGIPDFFKQSFPEGFTWERVTRYEDGGVVTVMQDTSLEDGCLVYHVQVRGVNFPNSNGPVMQKKTGWEPNTEMMYPADGGLRGYTHMALKVDGGGHLSCSFVTTYRSKKTGVGNIKM PGIHAVDHRLERLEESDNEMFVQREHAVAKFAGLGGGMDLYKGGSGSEPKSSDKTHTCPPCPAPELLGGPSVFLFPPKPKDTLMISRTPEVTCVVDVSHEDPEVKFNWYVDGVEVHNAKTKPREEQYNSTYRVVSVLTVLHQDWLNGKEYKCKVSNKALPAPIEKTISKAKGQPREPQVYTLPPSRDELTKNQVSLTCLVKGFYPSDIAVEWESNGQPENNYKTPPVLDSDGSFFLYSKLTVDKSRWQQGNVFSCSVMHEALHNHYTQKSLSLSPGK
A1F-Fc	METDTLLLWVLLLWVPGSTGKAELASEKPFRCADVYQAGFNKSGIYIYINMPEPKVFCNMDVNGGGWTVIQHREDGSLDFQRGWKEYKMGFGNPSGEYWLGNFIFAITSQRQYMLRIELMDWEGNRAYSQYDRFHIGNEKQNYRLYLKGHTGTAGKQSSILHGAADFSTKDADNDNCMCKCALMLTGGWWFDACGPSNLNGMFYTAGQNHGKLNIGIKWHYFKGPSYSLRSTTMMIRPLDFGGSGSEPKSSDKTHTCPPCPAPELLGGPSVFLFPPKPKDTLMISRTPEVTCVVDVSHEDPEVKFNWYVDGVEVHNAKTKPREEQYNSTYRVVSVLTVLHQDWLNGKEYKCKVSNKALPAPIEKTISKAKGQPREPQVYTLPPSRDELTKNQVSLTCLVKGFYPSDIAVEWESNGQPENNYKTPPVLDSDGSFFLYSKLTVDKSRWQQGNVFSCSVMHEALHNHYTQKSLSLSPGKGGSHHHHHH

5

10

15

20

25

**Supplementary Materials 1. Geometry specification in the .config files used in fusion protocol (using the WORMS protocol at <https://github.com/willsheffler/worms>).**

**D2 Dihedron:**

5 [('fc\_binder',orient(None,'C')),('Monomer',orient('N','C')),('C2\_N',orient('N',None))]  
D2(c2=0, c2b=-1)

**D3 Dihedron:**

10 [('fc\_binder',orient(None,'C')),('Monomer',orient('N','C')),('C3\_N',orient('N',None))]  
D3(c2=0, c2b=-1)

**T32 Tetrahedron:**

15 [('fc\_binder',orient(None,'C')),('Monomer',orient('N','C')),('C3\_N',orient('N',None))]  
Tetrahedral(c2=0, c3=-1)

**O32 Octahedron:**

[('fc\_binder',orient(None,'C')),('Monomer',orient('N','C')),('C3\_N',orient('N',None))]  
Octahedral(c2=0, c3=-1)

20 **O42 Octahedron:**

[('fc\_binder',orient(None,'C')),('Monomer',orient('N','C')),('C4\_N',orient('N',None))]  
Octahedral(c2=0, c4=-1)

**I32 Icosahedron:**

25 [('fc\_binder',orient(None,'C')),('Monomer',orient('N','C')),('C3\_N',orient('N',None))]  
Icosahedral(c2=0, c3=-1)

**I52 Icosahedron:**

30 [('fc\_binder',orient(None,'C')),('Monomer',orient('N','C')),('C5\_N',orient('N',None))]  
Icosahedral(c2=0, c5=-1)

35

40

**Supplementary Materials 2. Example .json file database entry for each building block used in the helical fusion protocol (using the WORMS protocol at <https://github.com/willsheffler/worms>).**

```
5      [
      {"file": "/path/to/fc_binder/file1.pdb",
       "name": "protein_a_d_domain" ,
       "class": ["fc_binder"],
       "type": "fc_binder" ,
10      "connections": [
          {"chain": 1, "direction": "C", "residues":["-17:"]}
      ]
    },

15      {"file": "/path/to/monomer/file1.pdb",
       "name": "dhr10" ,
       "class": ["monomer"],
       "type": "monomer" ,
       "connections": [
20      {"chain": 1, "direction": "N", "residues":[":50"]},
          {"chain": 1, "direction": "C", "residues":["-150:"]}
      ]
    },

25      {"file": "/path/to/cyclic_oligomer/file1.pdb",
       "name": "example_c2" ,
       "class": ["C2_N"],
       "type": "C2_N" ,
       "connections": [
30      {"chain": 1, "direction": "N", "residues":[":50"]},
      ]
    },

35      {"file": "/path/to/cyclic_oligomer/file2.pdb",
       "name": "example_c3" ,
       "class": ["C3_N"],
       "type": "C3_N" ,
       "connections": [
40      {"chain": 1, "direction": "N", "residues":[":50"]},
      ]
    }
  ]

45
```

**Supplementary Materials 3. Example command line command used to launch AbC fusion generation job (using the WORMS protocol at <https://github.com/willsheffler/worms>).**

5 PYTHONPATH="/home/rdd48/worms" python /path/to/generate\_chains.py --config\_file  
/path/to/config\_file/see\_fig\_s2 --err\_cutoff 0.5 --clash\_cutoff 1.0 --database\_files  
/path/to/database\_files/see\_fig\_s1

10

15

20

25

30

35

40

45

**Supplementary Materials 4. Example .xml file used during post-helical fusion residue design.** Paths to designable residue files (resfiles) and symdef (symmetry definition) files provided on the command-line during the run.

```
5 <ROSETTASCRIPTS>
  <SCOREFXNS>
    <ScoreFunction name="sfx_hard_symm" weights="beta.wts" symmetric="1" >
      <Reweight scoretype="res_type_constraint" weight="1.0" />
      <Reweight scoretype="aa_composition" weight="1.0" />
10     <Reweight scoretype="coordinate_constraint" weight="1.00" />
    </ScoreFunction>
  </SCOREFXNS>
  <TASKOPERATIONS>
    <InitializeFromCommandline name="init" />
    <IncludeCurrent name="ic" />
    <RestrictIdentities name="nomutate_VIRTUAL" identities="XXX" prevent_repacking="1" />
    <LimitAromaChi2 name="limitaro" chi2max="110" chi2min="70" />
    <ReadResfile name="resfile_designable" filename="%%resfile%%" />
15  </TASKOPERATIONS>
  <MOVERS>
    <SetupForSymmetry name="symmetry_setup" definition="%%symdef%%"></SetupForSymmetry>
    <SymPackRotamersMover name="design_rotamers_resfile" scorefxn="sfx_hard_symm"
20 task_operations="init,ic,limitaro,nomutate_VIRTUAL,resfile_designable"></SymPackRotamersMover>
  </MOVERS>
  <PROTOCOLS>
    <Add mover_name="symmetry_setup" />
    <Add mover_name="design_rotamers_resfile" />
  </PROTOCOLS>
30 </ROSETTASCRIPTS>

35

40

45
```



**Supplementary Materials 5. Example resfile (residue specification file) used to design AbC helical fusion outputs.** Designable residues were near the fusion junctions. Residues from the original building were occasionally restored by directly specifying them (e.g. residue 245 was a glutamate in the original building block).

5

NATRO

START

245 A PIKAA E

248 A PIKAA R

10 253 A APOLAR

265 A PIKAA D

272 A PIKAA AVIL

277 A PIKAA VIL

294 A PIKAA E

15 298 A PIKAA S

306 A APOLAR

307 A PIKAA AVIL

309 A APOLAR

311 A PIKAA ST

20

25

30

## Full References

1. R.-M. Lu, Y.-C. Hwang, I.-J. Liu, C.-C. Lee, H.-Z. Tsai, H.-J. Li, H.-C. Wu, Development of therapeutic antibodies for the treatment of diseases. *J. Biomed. Sci.* **27**, 1–30 (2020).
- 5 2. A. M. Cuesta, N. Sainz-Pastor, J. Bonet, B. Oliva, L. Alvarez-Vallina, Multivalent antibodies: when design surpasses evolution. *Trends Biotechnol.* **28**, 355–362 (2010).
3. N. Nuñez-Prado, M. Compte, S. Harwood, A. Álvarez-Méndez, S. Lykkemark, L. Sanz, L. Álvarez-Vallina, The coming of age of engineered multivalent antibodies. *Drug Discov. Today.* **20**, 588–594 (2015).
- 10 4. N. S. Laursen, R. H. E. Friesen, X. Zhu, M. Jongeneelen, S. Blokland, J. Vermond, A. van Eijgen, C. Tang, H. van Diepen, G. Obmolova, M. van der Neut Kofschoten, D. Zuijdgéest, R. Straetemans, R. M. B. Hoffman, T. Nieusma, J. Pallesen, H. L. Turner, S. M. Bernard, A. B. Ward, J. Luo, L. L. M. Poon, A. P. Tretiakova, J. M. Wilson, M. P. Limberis, R. Vogels, B. Brandenburg, J. A. Kolkman, I. A. Wilson, Universal protection against influenza infection by a multidomain antibody to influenza hemagglutinin. *Science.* **362**, 598–602 (2018).
- 15 5. O. Seifert, A. Plappert, S. Fellermeier, M. Siegemund, K. Pfizenmaier, R. E. Kontermann, Tetravalent antibody-scTRAIL fusion proteins with improved properties. *Mol. Cancer Ther.* **13**, 101–111 (2014).
- 20 6. T. F. Rowley, S. J. Peters, M. Aylott, R. Griffin, N. L. Davies, L. J. Healy, R. M. Cutler, A. Eddleston, T. L. Pither, J. M. Sopp, O. Zaccaro, G. Fossati, K. Cain, A. M. Ventom, H. Hailu, E. J. Ward, J. Sherington, F. R. Brennan, F. Fallah-Arani, D. P. Humphreys, Engineered hexavalent Fc proteins with enhanced Fc-gamma receptor avidity provide insights into immune-complex interactions. *Commun Biol.* **1**, 146 (2018).
- 25 7. R. S. Riley, E. S. Day, Frizzled7 Antibody-Functionalized Nanoshells Enable Multivalent Binding for Wnt Signaling Inhibition in Triple Negative Breast Cancer Cells. *Small.* **13** (2017), doi:10.1002/smll.201700544.
8. H. J. Kang, Y. J. Kang, Y.-M. Lee, H.-H. Shin, S. J. Chung, S. Kang, Developing an antibody-binding protein cage as a molecular recognition drug modular nanoplatform. *Biomaterials.* **33**, 5423–5430 (2012).
- 30 9. H. Kim, Y. J. Kang, J. Min, H. Choi, S. Kang, Development of an antibody-binding modular nanoplatform for antibody-guided targeted cell imaging and delivery. *RSC Advances.* **6** (2016), pp. 19208–19213.
10. S. I. Lim, C. I. Lukianov, J. A. Champion, Self-assembled protein nanocarrier for intracellular delivery of antibody. *J. Control. Release.* **249**, 1–10 (2017).
- 35 11. K. Uhde-Holzem, M. McBurney, B. D. B. Tiu, R. C. Advincula, R. Fischer, U. Commandeur, N. F. Steinmetz, Production of Immunoabsorbent Nanoparticles by Displaying Single-Domain Protein A on Potato Virus X. *Macromol. Biosci.* **16**, 231–241 (2016).
12. A. Miller, S. Carr, T. Rabbits, H. Ali, Multimeric antibodies with increased valency surpassing functional affinity and potency thresholds using novel formats. *MAbs.* **12**, 1752529 (2020).

13. E. Rujas, I. Kucharska, Y. Z. Tan, S. Benlekbir, H. Cui, T. Zhao, G. A. Wasney, P. Budyłowski, F. Guvenc, J. C. Newton, T. Sicard, A. Semesi, K. Muthuraman, A. Nouanesengsy, K. Prieto, S. A. Bueler, S. Youssef, S. Liao-Chan, J. Glanville, N. Christie-Holmes, S. Mubareka, S. D. Gray-Owen, J. L. Rubinstein, B. Treanor, J.-P. Julien, Multivalency transforms SARS-CoV-2 antibodies into broad and ultrapotent neutralizers, ,  
5 doi:10.1101/2020.10.15.341636.
14. I. Vulovic, Q. Yao, Y.-J. Park, A. Courbet, A. Norris, F. Busch, A. Sahasrabudde, H. Merten, D. D. Sahtoe, G. Ueda, J. A. Fallas, S. J. Weaver, Y. Hsia, R. A. Langan, A. Plückthun, V. H. Wysocki, D. Veessler, G. J. Jensen, D. Baker, Generation of ordered  
10 protein assemblies using rigid three-body fusion. *bioRxiv* (2020), p. 2020.07.18.210294.
15. Y. Hsia, R. Mout, W. Sheffler, N. I. Edman, I. Vulovic, Y.-J. Park, R. L. Redler, M. J. Bick, A. K. Bera, A. Courbet, A. Kang, T. J. Brunette, U. Nattermann, E. Tsai, A. Saleem, C. M. Chow, D. Ekiert, G. Bhabha, D. Veessler, D. Baker, Hierarchical design of multi-scale protein  
15 complexes by combinatorial assembly of oligomeric helical bundle and repeat protein building blocks (2020).
16. J. B. Bale, S. Gonen, Y. Liu, W. Sheffler, D. Ellis, C. Thomas, D. Cascio, T. O. Yeates, T. Gonen, N. P. King, D. Baker, Accurate design of megadalton-scale two-component icosahedral protein complexes. *Science*. **353**, 389–394 (2016).
17. G. Ueda, A. Antanasijevic, J. A. Fallas, W. Sheffler, J. Copps, D. Ellis, G. Hutchinson, A. Moyer, A. Yasmeen, Y. Tsybovsky, Y.-J. Park, M. J. Bick, B. Sankaran, R. A. Gillespie, P. J. M. Brouwer, P. H. Zwart, D. Veessler, M. Kanekiyo, B. S. Graham, R. Sanders, J. P. Moore, P. J. Klasse, A. B. Ward, N. King, D. Baker, Tailored Design of Protein Nanoparticle  
20 Scaffolds for Multivalent Presentation of Viral Glycoprotein Antigens. *bioRxiv* (2020), p. 2020.01.29.923862.
18. M. Graille, E. A. Stura, A. L. Corper, B. J. Sutton, M. J. Taussig, J. B. Charbonnier, G. J. Silverman, Crystal structure of a *Staphylococcus aureus* protein A domain complexed with the Fab fragment of a human IgM antibody: structural basis for recognition of B-cell  
25 receptors and superantigen activity. *Proc. Natl. Acad. Sci. U. S. A.* **97**, 5399–5404 (2000).
19. T. J. Brunette, F. Parmeggiani, P.-S. Huang, G. Bhabha, D. C. Ekiert, S. E. Tsutakawa, G. L. Hura, J. A. Tainer, D. Baker, Exploring the repeat protein universe through computational  
30 protein design. *Nature*. **528**, 580–584 (2015).
20. J. A. Fallas, G. Ueda, W. Sheffler, V. Nguyen, D. E. McNamara, B. Sankaran, J. H. Pereira, F. Parmeggiani, T. J. Brunette, D. Cascio, T. R. Yeates, P. Zwart, D. Baker, Computational design of self-assembling cyclic protein homo-oligomers. *Nat. Chem.* **9**, 353–360 (2017).
21. P.-S. Huang, G. Oberdorfer, C. Xu, X. Y. Pei, B. L. Nannenga, J. M. Rogers, F. DiMaio, T. Gonen, B. Luisi, D. Baker, High thermodynamic stability of parametrically designed helical  
35 bundles. *Science*. **346**, 481–485 (2014).
22. T. O. Yeates, Y. Liu, J. Laniado, The design of symmetric protein nanomaterials comes of age in theory and practice. *Curr. Opin. Struct. Biol.* **39**, 134–143 (2016).
23. B. M. Baynes, D. I. C. Wang, B. L. Trout, Role of arginine in the stabilization of proteins  
40 against aggregation. *Biochemistry*. **44**, 4919–4925 (2005).

24. D. Schneidman-Duhovny, M. Hammel, J. A. Tainer, A. Sali, Accurate SAXS profile computation and its assessment by contrast variation experiments. *Biophys. J.* **105**, 962–974 (2013).
- 5 25. K. N. Dyer, M. Hammel, R. P. Rambo, S. E. Tsutakawa, I. Rodic, S. Classen, J. A. Tainer, G. L. Hura, High-throughput SAXS for the characterization of biomolecules in solution: a practical approach. *Methods Mol. Biol.* **1091**, 245–258 (2014).
- 10 26. K. Mohan, G. Ueda, A. R. Kim, K. M. Jude, J. A. Fallas, Y. Guo, M. Hafer, Y. Miao, R. A. Saxton, J. Piehler, V. G. Sankaran, D. Baker, K. C. Garcia, Topological control of cytokine receptor signaling induces differential effects in hematopoiesis. *Science*. **364** (2019), doi:10.1126/science.aav7532.
- 15 27. M. Siegemund, F. Schneider, M. Hutt, O. Seifert, I. Müller, D. Kulms, K. Pfizenmaier, R. E. Kontermann, IgG-single-chain TRAIL fusion proteins for tumour therapy. *Sci. Rep.* **8**, 1–11 (2018).
- 20 28. J. D. Graves, J. J. Kordich, T.-H. Huang, J. Piasecki, T. L. Bush, T. Sullivan, I. N. Foltz, W. Chang, H. Douangpanya, T. Dang, J. W. O’Neill, R. Mallari, X. Zhao, D. G. Branstetter, J. M. Rossi, A. M. Long, X. Huang, P. M. Holland, Apo2L/TRAIL and the death receptor 5 agonist antibody AMG 655 cooperate to promote receptor clustering and antitumor activity. *Cancer Cell*. **26**, 177–189 (2014).
- 25 29. J. Naval, D. de Miguel, A. Gallego-Lleyda, A. Anel, L. Martinez-Lostao, Importance of TRAIL Molecular Anatomy in Receptor Oligomerization and Signaling. Implications for Cancer Therapy. *Cancers* . **11** (2019), doi:10.3390/cancers11040444.
- 30 30. D. de Miguel, J. Lemke, A. Anel, H. Walczak, L. Martinez-Lostao, Onto better TRAILS for cancer treatment. *Cell Death Differ.* **23**, 733–747 (2016).
- 35 31. M. H. Tuthill, A. Montinaro, J. Zinngrebe, K. Prieske, P. Draber, S. Prieske, T. Newsom-Davis, S. von Karstedt, J. Graves, H. Walczak, TRAIL-R2-specific antibodies and recombinant TRAIL can synergise to kill cancer cells. *Oncogene*. **34** (2015), pp. 2138–2144.
- 30 32. V.-M. Leppänen, P. Saharinen, K. Alitalo, Structural basis of Tie2 activation and Tie2/Tie1 heterodimerization. *Proc. Natl. Acad. Sci. U. S. A.* **114**, 4376–4381 (2017).
- 35 33. Y. T. Zhao, J. A. Fallas, S. Saini, G. Ueda, L. Somasundaram, Z. Zhou, I. Xavier, D. Ehnes, C. Xu, L. Carter, S. Wrenn, J. Mathieu, D. L. Sellers, D. Baker, H. Ruohola-Baker, F-domain valency determines outcome of signaling through the angiopoietin pathway. *Cold Spring Harbor Laboratory* (2020), p. 2020.09.19.304188.
- 40 34. R. S. Kornbluth, M. Stempniak, G. W. Stone, Design of CD40 agonists and their use in growing B cells for cancer immunotherapy. *Int. Rev. Immunol.* **31**, 279–288 (2012).
- 35 35. R. H. Vonderheide, M. J. Glennie, Agonistic CD40 Antibodies and Cancer Therapy. *Clinical Cancer Research*. **19** (2013), pp. 1035–1043.
- 40 36. E. R. Steenblock, S. H. Wrzesinski, R. A. Flavell, T. M. Fahmy, Antigen presentation on artificial acellular substrates: modular systems for flexible, adaptable immunotherapy. *Expert Opin. Biol. Ther.* **9**, 451–464 (2009).

37. J. V. Kim, J.-B. Latouche, I. Rivière, M. Sadelain, The ABCs of artificial antigen presentation. *Nat. Biotechnol.* **22**, 403–410 (2004).
38. E. Seydoux, L. J. Homad, A. J. MacCamy, K. R. Parks, N. K. Hurlburt, M. F. Jennewein, N. R. Akins, A. B. Stuart, Y.-H. Wan, J. Feng, R. E. Whaley, S. Singh, M. Boeckh, K. W. Cohen, M. J. McElrath, J. A. Englund, H. Y. Chu, M. Pancera, A. T. McGuire, L. Stamatatos, Analysis of a SARS-CoV-2-Infected Individual Reveals Development of Potent Neutralizing Antibodies with Limited Somatic Mutation. *Immunity*. **53**, 98–105.e5 (2020).
39. C. Wang, W. Li, D. Drabek, N. M. A. Okba, R. van Haperen, A. D. M. E. Osterhaus, F. J. M. van Kuppeveld, B. L. Haagmans, F. Grosveld, B.-J. Bosch, A human monoclonal antibody blocking SARS-CoV-2 infection. *Nat. Commun.* **11**, 2251 (2020).
40. M. A. Tortorici, M. Beltramello, F. A. Lempp, D. Pinto, H. V. Dang, L. E. Rosen, M. McCallum, J. Bowen, A. Minola, S. Jaconi, F. Zatta, A. De Marco, B. Guarino, S. Bianchi, E. J. Lauron, H. Tucker, J. Zhou, A. Peter, C. Havenar-Daughton, J. A. Wojcechowskyj, J. B. Case, R. E. Chen, H. Kaiser, M. Montiel-Ruiz, M. Meury, N. Czudnochowski, R. Spreafico, J. Dillen, C. Ng, N. Sprugasci, K. Culap, F. Benigni, R. Abdelnabi, S.-Y. C. Foo, M. A. Schmid, E. Cameroni, A. Riva, A. Gabrieli, M. Galli, M. S. Pizzuto, J. Neyts, M. S. Diamond, H. W. Virgin, G. Snell, D. Corti, K. Fink, D. Veessler, Ultrapotent human antibodies protect against SARS-CoV-2 challenge via multiple mechanisms. *Science* (2020), doi:10.1126/science.abe3354.
41. L. Piccoli, Y.-J. Park, M. A. Tortorici, N. Czudnochowski, A. C. Walls, M. Beltramello, C. Silacci-Fregni, D. Pinto, L. E. Rosen, J. E. Bowen, O. J. Acton, S. Jaconi, B. Guarino, A. Minola, F. Zatta, N. Sprugasci, J. Bassi, A. Peter, A. De Marco, J. C. Nix, F. Mele, S. Jovic, B. F. Rodriguez, S. V. Gupta, F. Jin, G. Piumatti, G. Lo Presti, A. F. Pellanda, M. Biggiogero, M. Tarkowski, M. S. Pizzuto, E. Cameroni, C. Havenar-Daughton, M. Smithey, D. Hong, V. Lepori, E. Albanese, A. Ceschi, E. Bernasconi, L. Elzi, P. Ferrari, C. Garzoni, A. Riva, G. Snell, F. Sallusto, K. Fink, H. W. Virgin, A. Lanzavecchia, D. Corti, D. Veessler, Mapping Neutralizing and Immunodominant Sites on the SARS-CoV-2 Spike Receptor-Binding Domain by Structure-Guided High-Resolution Serology. *Cell*. **183**, 1024–1042.e21 (2020).
42. D. Pinto, Y.-J. Park, M. Beltramello, A. C. Walls, M. A. Tortorici, S. Bianchi, S. Jaconi, K. Culap, F. Zatta, A. De Marco, A. Peter, B. Guarino, R. Spreafico, E. Cameroni, J. B. Case, R. E. Chen, C. Havenar-Daughton, G. Snell, A. Telenti, H. W. Virgin, A. Lanzavecchia, M. S. Diamond, K. Fink, D. Veessler, D. Corti, Cross-neutralization of SARS-CoV-2 by a human monoclonal SARS-CoV antibody. *Nature*. **583**, 290–295 (2020).
43. A. C. Walls, Y.-J. Park, M. A. Tortorici, A. Wall, A. T. McGuire, D. Veessler, Structure, Function, and Antigenicity of the SARS-CoV-2 Spike Glycoprotein. *Cell*. **181**, 281–292.e6 (2020).
44. E. Hiramoto, A. Tsutsumi, R. Suzuki, S. Matsuoka, S. Arai, M. Kikkawa, T. Miyazaki, The IgM pentamer is an asymmetric pentagon with an open groove that binds the AIM protein. *Sci Adv.* **4**, eaau1199 (2018).
45. E. E. Idusogie, L. G. Presta, H. Gazzano-Santoro, K. Totpal, P. Y. Wong, M. Ultsch, Y. G. Meng, M. G. Mulkerrin, Mapping of the C1q binding site on rituxan, a chimeric antibody with a human IgG1 Fc. *J. Immunol.* **164**, 4178–4184 (2000).

46. F. DiMaio, N. Echols, J. J. Headd, T. C. Terwilliger, P. D. Adams, D. Baker, Improved low-resolution crystallographic refinement with Phenix and Rosetta. *Nature Methods*. **10** (2013), pp. 1102–1104.
- 5 47. E. T. Boder, K. D. Wittrup, Optimal screening of surface-displayed polypeptide libraries. *Biotechnol. Prog.* **14**, 55–62 (1998).
48. F. W. Studier, F. William Studier, Protein production by auto-induction in high-density shaking cultures. *Protein Expression and Purification*. **41** (2005), pp. 207–234.
- 10 49. J. K. Leman, B. D. Weitzner, S. M. Lewis, J. Adolf-Bryfogle, N. Alam, R. F. Alford, M. Aprahamian, D. Baker, K. A. Barlow, P. Barth, B. Basanta, B. J. Bender, K. Blacklock, J. Bonet, S. E. Boyken, P. Bradley, C. Bystroff, P. Conway, S. Cooper, B. E. Correia, B. Coventry, R. Das, R. M. De Jong, F. DiMaio, L. Dsilva, R. Dunbrack, A. S. Ford, B. Frenz, D. Y. Fu, C. Geniesse, L. Goldschmidt, R. Gowthaman, J. J. Gray, D. Gront, S. Guffy, S. Horowitz, P.-S. Huang, T. Huber, T. M. Jacobs, J. R. Jeliazkov, D. K. Johnson, K. Kappel, J. Karanicolas, H. Khakzad, K. R. Khar, S. D. Khare, F. Khatib, A. Khramushin, I. C. King, 15 R. Kleffner, B. Koepnick, T. Kortemme, G. Kuenze, B. Kuhlman, D. Kuroda, J. W. Labonte, J. K. Lai, G. Lapidoth, A. Leaver-Fay, S. Lindert, T. Linsky, N. London, J. H. Lubin, S. Lyskov, J. Maguire, L. Malmström, E. Marcos, O. Marcu, N. A. Marze, J. Meiler, R. Moretti, V. K. Mulligan, S. Nerli, C. Norn, S. Ó'Conchúir, N. Ollikainen, S. Ovchinnikov, M. S. Pacella, X. Pan, H. Park, R. E. Pavlovicz, M. Pethe, B. G. Pierce, K. B. Pilla, B. Raveh, P. 20 Douglas Renfrew, S. S. Roy Burman, A. Rubenstein, M. F. Sauer, A. Scheck, W. Schief, O. Schueler-Furman, Y. Sedan, A. M. Sevy, N. G. Sgourakis, L. Shi, J. B. Siegel, D.-A. Silva, S. Smith, Y. Song, A. Stein, M. Szegedy, F. D. Teets, S. B. Thyme, R. Y.-R. Wang, A. Watkins, L. Zimmerman, R. Bonneau, Macromolecular modeling and design in Rosetta: recent methods and frameworks. *Nat. Methods*. **17**, 665–680 (2020).
- 25 50. D. H. Barouch, Z.-Y. Yang, W.-P. Kong, B. Koriath-Schmitz, S. M. Sumida, D. M. Truitt, M. G. Kishko, J. C. Arthur, A. Miura, J. R. Mascola, N. L. Letvin, G. J. Nabel, A human T-cell leukemia virus type 1 regulatory element enhances the immunogenicity of human immunodeficiency virus type 1 DNA vaccines in mice and nonhuman primates. *J. Virol.* **79**, 8828–8834 (2005).
- 30 51. D. Corti, S. Bianchi, F. Vanzetta, A. Minola, L. Perez, G. Agatic, B. Guarino, C. Silacci, J. Marcandalli, B. J. Marsland, A. Piralla, E. Percivalle, F. Sallusto, F. Baldanti, A. Lanzavecchia, Cross-neutralization of four paramyxoviruses by a human monoclonal antibody. *Nature*. **501**, 439–443 (2013).
- 35 52. C. Suloway, J. Pulokas, D. Fellmann, A. Cheng, F. Guerra, J. Quispe, S. Stagg, C. S. Potter, B. Carragher, Automated molecular microscopy: the new Legion system. *J. Struct. Biol.* **151**, 41–60 (2005).
- 40 53. G. C. Lander, S. M. Stagg, N. R. Voss, A. Cheng, D. Fellmann, J. Pulokas, C. Yoshioka, C. Irving, A. Mulder, P.-W. Lau, D. Lyumkis, C. S. Potter, B. Carragher, Appion: an integrated, database-driven pipeline to facilitate EM image processing. *J. Struct. Biol.* **166**, 95–102 (2009).
54. T. Grant, A. Rohou, N. Grigorieff, TEM, user-friendly software for single-particle image processing. *Elife*. **7** (2018), doi:10.7554/eLife.35383.
55. K. Zhang, Gctf: Real-time CTF determination and correction. *J. Struct. Biol.* **193**, 1–12

(2016).

56. A. Punjani, J. L. Rubinstein, D. J. Fleet, M. A. Brubaker, cryoSPARC: algorithms for rapid unsupervised cryo-EM structure determination. *Nat. Methods*. **14**, 290–296 (2017).
57. D. Tegunov, P. Cramer, Real-time cryo-electron microscopy data preprocessing with Warp. *Nat. Methods*. **16**, 1146–1152 (2019).
58. S. H. W. Scheres, S. Chen, Prevention of overfitting in cryo-EM structure determination. *Nat. Methods*. **9**, 853–854 (2012).
59. P. B. Rosenthal, R. Henderson, Optimal determination of particle orientation, absolute hand, and contrast loss in single-particle electron cryomicroscopy. *J. Mol. Biol.* **333**, 721–745 (2003).
60. S. Chen, G. McMullan, A. R. Faruqi, G. N. Murshudov, J. M. Short, S. H. W. Scheres, R. Henderson, High-resolution noise substitution to measure overfitting and validate resolution in 3D structure determination by single particle electron cryomicroscopy. *Ultramicroscopy*. **135**, 24–35 (2013).
61. K. L. DeCicco-Skinner, G. H. Henry, C. Cataisson, T. Tabib, J. C. Gwilliam, N. J. Watson, E. M. Bullwinkle, L. Falkenburg, R. C. O’Neill, A. Morin, J. S. Wiest, Endothelial cell tube formation assay for the in vitro study of angiogenesis. *J. Vis. Exp.*, e51312 (2014).
62. K. H. D. Crawford, R. Eguia, A. S. Dingens, A. N. Loes, K. D. Malone, C. R. Wolf, H. Y. Chu, M. A. Tortorici, D. Veessler, M. Murphy, D. Pettie, N. P. King, A. B. Balazs, J. D. Bloom, Protocol and Reagents for Pseudotyping Lentiviral Particles with SARS-CoV-2 Spike Protein for Neutralization Assays. *Viruses*. **12** (2020), doi:10.3390/v12050513.

25